Thin Solid Films 579 (2015) 174–198

Contents lists available at ScienceDirect

Thin Solid Films

journal homepage: www.elsevier.com/locate/tsf

Critical review

The use of hollow cathodes in deposition processes: A critical review

Stephen Muhl *, Argelia Pérez

Instituto de Investigaciones en Materiales, Universidad Nacional Autónoma de México, Ciudad Universitaria, Coyoacán, A.P. 70-360, C.P. 04510, México D.F., Mexico

ARTICLE INFO

Available online 3 March 2015

Keywords:
Hollow cathode
Gas flow sputtering
Plasmas
Thin films

ABSTRACT

The first report of a discharge in a hollow cathode was by F. Paschen in 1916. That study showed that such a system was capable of producing a high electron flux and relatively low ion and neutral temperatures. About 40 years later, the work of Lidsky and others showed that hollow cathode arc discharges were one of the best plasma sources available at that time. The term "hollow cathode discharges" has commonly been used in reference to almost any discharge in a cathode with a cavity-like geometry, such that the plasma was enclosed or partially bound by the electrode walls that were at the cathode potential. Just as the magnetic field trapping of the electrons in a magnetron cathode results in an increase in the plasma density, in the hollow cathode, the reduced electron loss due to the geometry of the cathode also results in a higher plasma density. At least three types of discharge can be established in a hollow cathode. At low power and/or at relatively low gas pressures, the plasma is a "conventional" discharge characterized by low currents and medium to high voltages (we will call this a discharge in a hollow cathode or D-HC). Even this type of plasma has a higher density than a normal planar parallel-plate or magnetron system because the hollow geometry strongly reduces the loss of electrons. Using an adequate combination of gas pressure and applied power with a given hollow cathode diameter, or separation of the cathode surface, the negative glow of the plasma can expand to occupy the majority of the interior volume of the cathode. Under this condition the plasma current can, for the same voltage, be 100 to 1000 times the value of the "simple" D-HC discharge, and the plasma density is correspondingly larger (we call this a hollow cathode discharge or HCD). If the cathode is not cooled, the discharge can transform into a dispersed arc as the electrode temperature increases and thermal-field electron emission becomes an important additional source of electrons (we will call this a hollow cathode arc or HCA). The accepted explanation for the HCD phenomenon involves the existence of high-energy "pendulum" electrons, which are reflected from the sheaths on either side of the cathode; the long trajectory of this electron is understood to produce a large number of secondary electrons, with this resulting in the high plasma density and plasma current. We describe the structure of a parallel-plate discharge, particularly the gas phase and cathode surface excitation and ionization collision processes. Using this description, we discuss some of the problems associated with the conventional hollow cathode model and we propose a new explanation that has important implications for the physics and applications of hollow cathodes.

In the last section of this review, we describe how hollow cathodes have and can be used to deposit thin films and nanostructured coatings. We provide an extensive and approximately chronological listing of how hollow cathodes have been successfully used to deposit materials, mainly by sputtering and plasma enhanced chemical vapour deposition based techniques.

Contents

* Corresponding author.
E-mail address: muhl@unam.mx (S. Muhl).

http://dx.doi.org/10.1016/j.tsf.2015.02.066
0040-6090/

1. Introduction

The hollow cathode effect is generally understood to involve a lower than normal resistance plasma state. The hollow cathode discharge develops as the distance between opposing cathode surfaces, *d*, is reduced while the applied potential, V_{pl}, and gas pressure, *p*, are kept constant, or conversely for a given cathode geometry, as the gas pressure is increased such that "*d.p*" product is 1–10 Torr cm depending on the gas used. The schematic I–V characteristic shown in Fig. 1 demonstrates a typical dependence of the plasma current on the applied voltage for a given gas pressure and cathode geometry. However, as can be seen from many reports of the experimental I–V data, the transition into the hollow cathode state is often not so obvious, or does not occur [1–8].

Quite a number of hollow cathode systems have been developed and one important difference is between the hot and cold cathode versions [9]. We will see later in this study that a combined thermal-field emission process of electrons from the hot cathode surface in contact with the plasma is a very important source of electrons and strongly influences the characteristics of the plasma [10]. However, many of the basic phenomena involved in the plasma formation within the cathode are similar in all the forms of the hollow cathode, although the relative importance of each is different.

The first report of a hollow cathode was by F. Paschen in 1916 [11]. That study showed that the system was capable of producing a high electron flux together with a relatively low ion and neutral gas temperature. About 40 years later, the work of Lidsky showed that hollow cathode arc discharges were one of the best plasma sources available at that time [12]. The term "hollow cathode discharges" has commonly been applied to plasmas in a cathode with a cavity-like geometry, such that the plasma is enclosed or partially bound by the walls that are at the cathode potential [12–14]. Just as the magnetic field trapping of the electrons in a magnetron cathode results in an increase in the plasma density (10^8–10^{11} cm^{-3} for magnetron sputtering [15]), in the hollow cathode, electron trapping by the geometry of the cathode also results in a higher plasma density, 10^{11} to $>10^{13}$ cm^{-3} [16–19]. However, it is very important to distinguish between the three different types of discharges that can be established in a hollow cathode [20]. In general, at low powers and/or at relatively low gas pressures, the plasma is a "conventional" discharge characterized by low currents and medium to high voltages (in this work, we will call this a discharge in a hollow cathode or D-HC). Even this simple plasma has a higher density, 10^{10}–10^{11} cm^{-3}, than that of a normal planar parallel electrode system because the hollow geometry significantly reduces the loss of electrons [19,21,22]. As we describe in detail later in this study, for an appropriate combination of gas pressure and hollow cathode diameter, as the applied power is increased, the negative glow of the plasma formed in front of the cylindrical surface of the cathode can expand to almost completely occupy the interior volume of the cathode. Under this condition, the plasma current can, for the same applied voltage, be 100 to 1000 times the value seen for the "simple" D-HC discharge and the plasma density can correspondingly be much larger (we will call this a hollow cathode discharge or HCD) [13,21,23–25]. Finally, if the cathode is not cooled, the discharge can transform into a dispersed arc as the electrode temperature increases and thermal-field electron emission becomes an important additional source of electrons (we will call this a hollow cathode arc or HCA) [26–29].

The accepted explanation for the HCD phenomenon involves the existence of high energy "pendulum" electrons which are reflected from the sheaths on either side of the inside of the cathode; the long trajectory of these electron is understood to produce a large number of secondary electrons, with this producing the high plasma density and plasma current [20,30,31].

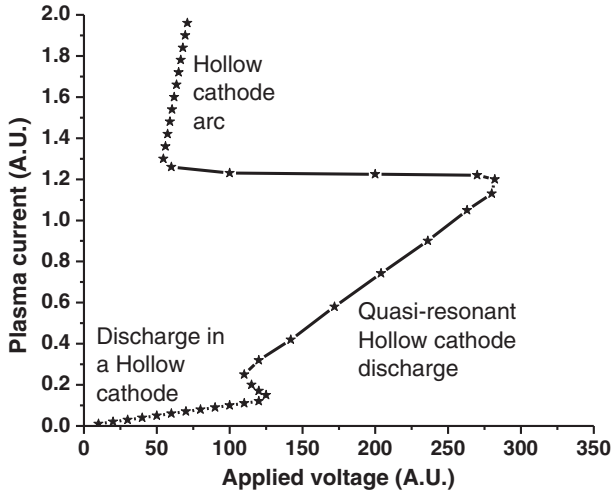

Fig. 1. A schematic drawing of the I–V characteristic of a hollow cathode system.

2. Gas discharges

As a prelude to the description of the most important plasma process that occur in hollow cathode discharges, we first present the basic definitions of the processes; interaction cross section, mean free path,

collision frequency, etc., together with a brief description of the typical structure of the gas discharge and the basic phenomenon that are important. In this way, the quasi-resonant hollow effect can be more clearly understood [32–38].

The particles that are involved in collisions in a plasma may be any of the following: electrons, neutral atoms or molecules, vibration and rotationally excited particles, ionized atoms or molecules or negative ions [15,39]. Each interaction between particle "a" and "b" can be described by the mean free path λ_{ab}, the average distance the particles "a" travel between collisions within the group of particles "b". The mean free path is given by,

$$\lambda_{ab} = {}^{1}\!/_{\sigma_{ab} n_b} \quad (1)$$

where σ_{ab} is the cross section of the interaction and n_b is the density of "b" particles. The collision or interaction cross section is given by [38],

$$\sigma_{ab} = \pi(r_a + r_b)^2. \quad (2)$$

Here, r_a and r_b are the real or effective radii of the particles for the given type of interaction.

The collision frequency ν_{ab} is the average rate in which two particles collide for a given system and is used to express the average number of collisions (interactions) per unit of time.

$$\nu_{ab} = n_a n_b (\sigma_{ab} V_a) = n_a n_b \pi (r_a + r_b)^2 V_a \quad (3)$$

Here, n_a and V_a are the density and speed of movement of the "a" particles, respectively. Frequently, the target "b" particles are considered to be at rest, but if the speed (energy) of the "b" particles is similar to that of the "a" particles, then the relative speed of the "a" to "b" particles must be used.

Obviously, the importance of any given interaction depends on the relative concentrations of the particles (where this is often dependent on the gas pressure), the collision cross-section (the size of the particles and the minimum interaction distance between them) and the relative speed (kinetic energy) of both types of particles.

Another important aspect of particle interactions is whether they are elastic or inelastic. In general, an elastic collision between particles of the same mass is a very efficient way to transfer energy within a group, but collisions between particles of very different masses are much less efficient. This is why for elastic collisions the small-mass electrons transfer little energy to the heavier particles, such as atoms and ions [35]. Similarly, if the pressure and the concentration of high energy ions are high, elastic collisions can rapidly increase the gas temperature [39,40]. One of the most important aspects of the pressure is that it controls whether the mean free path of the interaction is smaller, or larger, than the dimensions of the discharge.

In this description, we will not present the details of the mechanisms of the different types of collisions since this has been very well described in a variety of references such as [33,39]. What is of particular interest for the present work are the principal phenomena involved in the different types of processes that can occur in hollow cathode discharges and the dependence of these on the energy of the particles. In order to somewhat simplify our description, we will restrict our attention to interactions that involve gaseous atoms (Ar, He, vapours of cathode metal atoms, etc.) rather than molecules. Therefore, we will not consider vibrational, rotational or dissociation processes.

For hollow cathode discharges, the most important gas-phase particle interactions are relaxation, excitation, ionization, charge exchange, electron and ion impact generation of secondary electrons, photoemission of electrons, thermal and field emission of electrons and the combined thermal-field electron emission.

In the following, we will briefly describe the key points involved in the different interaction phenomena and then use that information to generate a clear phenomenological description of the hollow cathode discharges [41–43].

2.1. Elastic collisions

We know that plasmas consist of electrons, ions and neutral atoms, all of which are influenced, directly or indirectly, by the electric field. As stated earlier, the energy transfer between similar mass particles is very efficient, therefore the electrons quickly share their kinetic energy, but because of the difference in mass, the electrons do not efficiently increase the energy of the atoms and ions. The consequence of this is that electrons can easily absorb energy from the electric field, but the atoms and ions rapidly dissipate what energy they acquire to one another and to the electrodes in contact with the plasma. The gas temperature is normally similar to the temperature of the plasma container, but depends on the gas pressure and flow rate [44]. This can be very important for the hollow cathode since this is often effectively the gas container and the ion flux can make the cathode temperature very high, ≤1000 °C [45,46]. It should be noted that in elastic collisions between electrons and ions or atoms, the change of electron momentum is often large. Since for a hollow cathode there is only one direction for the electrons to "escape" from the plasma; along the axis of the cathode, the electron loss rate is less than for an equivalent parallel-plate discharge. This, in part, explains why high plasma densities can form in a hollow cathode discharge; we will discuss this in more detail later.

For typical average electron energies in these discharges (1–4 eV), the electron–ion collision cross section is approximately an order of magnitude larger than the electron-neutral cross section and therefore once the degree of ionization is greater than about 10%, electron–ion interactions can dominate the elastic energy electron collision processes [29,47], see Fig. 2.

Following the ideas described by several authors [15,35,36,48], the average fractional energy loss by an electron in an elastic collision with an argon atom or ion is a factor of ~10^{-4}. This is very different to the case of inelastic collisions where the electrons lose a relatively large amount of energy in each collision. It should be remembered that "cross section" is a convenient way to express the probability of a certain type of collision. Therefore, the importance of the various types of collisions, in terms of the energy loss of an electron, can be estimated from the product of the interaction cross section, the density of the target species and the energy loss per collision.

The plasma density, assuming that charge neutrality is conserved, is described as the number of electrons per unit volume, normally in cm^{-3}

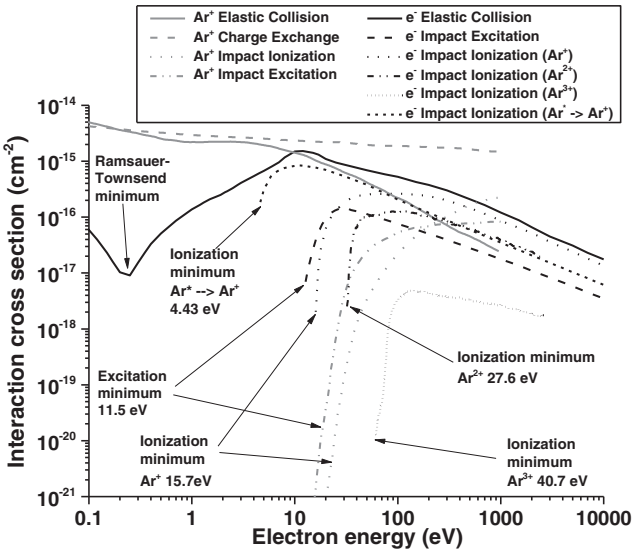

Fig. 2. Interaction cross sections for electron and ion impact processes [59,60].

or m^{-3}. The degree of plasma ionization I is the ratio of the plasma density to the gas density and can be calculated from Saha's equation,

$$I = \frac{n_e n_i}{n} = \left(\frac{\sqrt{2\pi m k}}{h}\right)^3 T^{3/2}\left(\exp\left(\frac{-eV_i}{kT}\right)\right) \quad (4)$$

in which n_e, n_i and n are respectively the densities of electrons, ions and neutral atoms, T is the absolute temperature, V_i is the ionization energy of the gas, m is atomic mass of the gas and the k is Boltzmann's constant [35,49].

2.2. Inelastic collisions

We will now review the details of the most relevant gas phase interactions that occur in hollow cathode discharges.

2.2.1. Atomic excitation

If the incident electron in a collision with a neutral atom has sufficient energy, it can cause elevation of outer-shell electrons to a higher energy, or excited state, see Eq. (5) [50]. The excited atom may return to the ground state through the radiative emission of a photon corresponding to the difference in the energy levels, and typically the lifetimes of such states are very short (~10^{-9} s) [51]. If the radiative transition to the ground sate is forbidden by quantum mechanics then the excited state is referred to as a metastable state and, since they can have long lifetimes (~10^{-3} s), they can carry their stored energy over quite large distances. Quite a few gases, such as Ar, He, Ne and N_2 have long-lived metastable states [34,35,52]. For argon the lifetime of the first metastable state is about 70 s [53]. There is an excitation cross section for each transition that is characteristic of a particular atom and typically the cross section rapidly increases above the threshold, for Ar 11.55 eV (see Table 1), corresponding to the metastable energy level and after reaching a broad maximum at approximately three times this energy, the probability then slowly decreases. Based on the reported cross section, for argon plasmas, the maximum in the probability of excitation is for electrons with energies of ~30 eV (cross section ~1.5×10^{-16} cm^{-2}), see Fig. 2 [34,54].

$$e^- + Ar \rightarrow Ar^* + e^- \quad (5)$$

Table 1 shows the ionization and metastable energies of various gases used in deposition processes [54,55].

The photons emitted during the de-excitation of the excited species can cause photoemission of electrons from the cathode material or from other gas species. Little information is available on the details of the formation of excited ions but it has been noted that the secondary electron emission coefficient of such excited ions can be considerably greater than that of non-excited ions when they are incident at the cathode [56,57].

Table 1
The first and second ionization energies and metastable energy levels of Ar, He, Ne, Kr and Xe [54,55].

First ionization energy (eV)		Second ionization energy (eV)	
Ar	15.76	Ar	27.63
He	24.59	He	54.42
Ne	21.59	Ne	40.96
Kr	14.0	Kr	24.36
Xe	12.13	Xe	20.97
Metastable energy levels (eV)/lifetime (s)			
Ar	11.55/~70		11.72/~40
He	19.82/9×10^3		20.61/2×10^{-2}
Ne	16.62/20		16.71/N.A.
Kr	9.91/2		9.99/1
Xe	8.31/~10		8.44/~10

2.2.2. Ionization

One of the most important gas-phase sources of electrons in plasmas is the electron impact ionization of neutral gas atoms [15].

$$e^- + Ar \rightarrow Ar^+ + 2e^- \quad (6)$$

The main difference between ionization and excitation by electron impact arises from the electrostatic interaction of the three charges after the collision process and this aspect has been addressed in detail by D. Rapp and P. Englander-Golden [58]. The principal result is that while the excitation maximum is close to the threshold, for ionization the difference in energy between maximum and threshold is typically a factor of four or five times that of the ionization energy. The cross-section maximum for ionization is also wider than that for excitation, see Fig. 2. Here it can be seen that for argon, the cross section for ionization by electron impact rises sharply from zero, at the threshold, by several orders of magnitude until it reaches a maximum of ~3×10^{-16} cm^{-2} at approximately 100 eV. For further increases of the electron energy, the cross section gradually decreases and at 500 eV, it is typically a factor of about two lower than the maximum value. However, the cross section is still large up to energies of several keV [15].

Additionally, ionization can take place for electron energies below the threshold for ionization if the target atom is in an excited metastable state [43]. The sum of the electron and excited state energies can be sufficient to cause ionization. However, there is little experimental data available to indicate the importance of this process. Ionization can also occur when two excited (metastable) atoms collide, but again good interaction cross section data is not available [34].

Although the threshold energy is higher, double ionization of Ar can be very important, as we will see later in this review. The maximum in the cross section for the formation of doubly ionized argon occurs at around 100 eV, but the value is slightly more than an order of magnitude smaller than for single ionization, see Fig. 2 [54].

Gas phase electron-ion recombination requires that a third-body be involved in the interaction. Modelling of the process,

$$e^- + Ar^+ + e^- \rightarrow Ar + e^- \quad (7)$$

for $T_e \gg T$ (where T_e is the electron temperature and T is either the gas or ion temperature depending on which is the largest), has shown that the rate constant of the process is proportional to the product $T_e^{-9/2} \times n_e$, where n_e is the plasma density. Therefore, for discharges with $T_e \geq 1$ eV and $n_e \leq 10^{13}$ cm^{-3} such a three-body recombination is not significant. The excessive energy of the recombination process is transferred to the kinetic energy of the free electron — the "third body". In this type of interaction heavy particles, ions, and neutrals are too slow and are ineffective as third-body partners [35,54]. For example, for recombination involving a noble gas atom, the coefficient of the three-body recombination process has been estimated to be $10^{-11} \times p$ cm^3 s^{-1}, where p is the gas pressure. Therefore, at a gas pressure of 1 Torr and a plasma density of 10^{11} cm^{-3}, the rate of the recombination process is about 10^{11} cm^{-3} s^{-1} which is approximately five orders of magnitude lower than the electron-impact ionization rate [61,62]. Consequently, in this study we assume that the recombination processes do not play a determinant role [34,35,63].

An important detail to bear in mind is that the similarities between the cross sections for electron induced excitation and ionization mean that where and when ionization occurs, excitation (light emission) also occurs. Conversely, in the parts of the plasma where there is little light emission, few ionization events occur.

Other gas phase interactions that can be important are those that occur between heavy particles; atomic excitation by ion impact, electron production by ion–atom impact (β-ionization) and simple charge transfer between ions and neutrals.

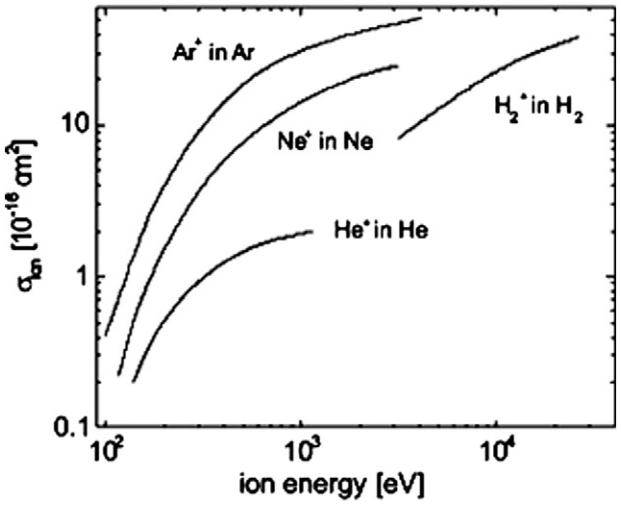

Fig. 3. The cross-section for electron production by ion–atom impact (β-ionization) for ions of the parent gas [15].

Fig. 3 shows a plot of the β-ionization cross-section versus ion energy for various combinations of gases and ions; basically, the cross section depends on the sizes of the atom and ion [15]. For ion energies of around 100 eV, the cross section for β-ionization is about an order of magnitude smaller than for electron impact ionization, but at 1 keV the ion cross section is slightly larger, see Figs. 2 and 3.

In high density plasmas where many excited metastable atoms/ions are generated, collisions between such excited species can also result in ionization and excitation [15,59],

$$Ar^* + Ar^* \rightarrow Ar^+ + Ar + e^- \quad (8)$$

$$e^- + Ar^* \rightarrow Ar^+ + 2e^- . \quad (9)$$

Here, the cross sections are similar to the atom–atom and electron–atom interaction cross sections, but the density of excited species determines the importance of this process.

Collisions between ions and neutral gas atoms can result in excitation of the gas atoms in a manner very similar to the electron–atom excitation process.

$$Ar^+ + Ar \rightarrow Ar^+ + Ar^*. \quad (10)$$

The energy threshold is the same for both types of impacting species, but the cross section for the ion-interaction is approximately an order of magnitude lower than for the electron process and the interaction reaches a maximum for ions with energies greater than 1 keV, see Fig. 3.

For charge transfer, the almost complete exchange of momentum is of importance. A collision between a rapidly moving ion and a slow atom can result in a slowly moving ion and a rapid neutral, where the components of velocity are conserved. If the colliding particles have the same mass, this process is very efficient and the collision is called *symmetric or resonant charge transfer*. The cross section for this process is comparable with that for elastic collisions, see Fig. 2, but the importance of the interaction obviously depends on the energy and the density of the ions. As can be seen, the cross section for resonant charge transfer is large at low collision energies, making this an important process in weakly ionized plasmas.

2.3. Cathode surface-related processes

We will now consider the details of the most relevant interactions that occur at the surface of the cathode. In this section, sputtering of the cathode by ion bombardment will not be dealt with since this mainly results in the emission of uncharged species [15,33,48,64].

2.3.1. Ion-impact-induced secondary-electron emission

Ions incident at the cathode surface can release electrons and this is of particular importance for all types of discharges [64,65]. The energy distribution of the emitted secondary electrons exhibits a broad maximum between 2 and 6 eV and is relatively independent of the kinetic energy of the incident ions [66,67]. To be able to emit an electron, the sum of the kinetic energy of the incident ion and the ionization potential of the gas atom, related to the ion, must be greater than twice the value of the work function of the material [15,33,35,68]. Furthermore, for every electron emitted from the surface, another is required to neutralize the incident ion. However, it has been observed that this is not always correct for Ne ions for which other relaxation processes play an important role [69].

Typical values of the ion-induced secondary electron yield, γ_{iee}, for singly charged argon are between 0.05 and 0.15 and normally the yield is considered to be almost independent of ion energy for energies <1 keV, see Fig. 4. The value of this coefficient depends strongly on the composition of the cathode, the crystal orientation of the material and the cleanness of the surface [15,70,71]. Additionally, the secondary electron yield for multiple charged ions is considerably larger; for Ar^{4+} $\gamma_{iee} \geq 1$ and for Ar^{2+} γ_{iee} ~0.5 and the energy of the emitted secondary electrons is higher; for Ar^{2+} from 2 to 12 eV [67,69,72–76].

In fact, it has been proposed that γ_{iee} is directly proportional to the corresponding ionization energy of the incident ion, as shown in Fig. 5 [66–68,77]. Here we have included published values of γ_{iee} for singly ionized Xe, Kr, Ar, Ne and He, together with doubly ionized Ar^{2+}, incident at pure polycrystalline Au. It should be noted that γ_{iee} for Ar^{2+} is approximately four times that of Ar^+. Furthermore, assuming that the linear relationship remains correct, it can be seen that γ_{iee} values for doubly ionized Ne and He would be approximately 0.8 and 1.15, respectively.

2.3.2. Ion reflection

The probability of ion reflection and the energy of the reflected particles depend on many factors, such as the mass of the incident ions and the target atoms, and the angle of incidence [78–80]. For typical sputtering conditions using argon and a transition metal target, between 40 and 50% of the ions accelerated by the sheath potential can rebound from the cathode surface as high energy neutral atoms [81]. If the conditions are such that atoms with high-energy are scattered from the cathode, then these can collide with the gas atoms

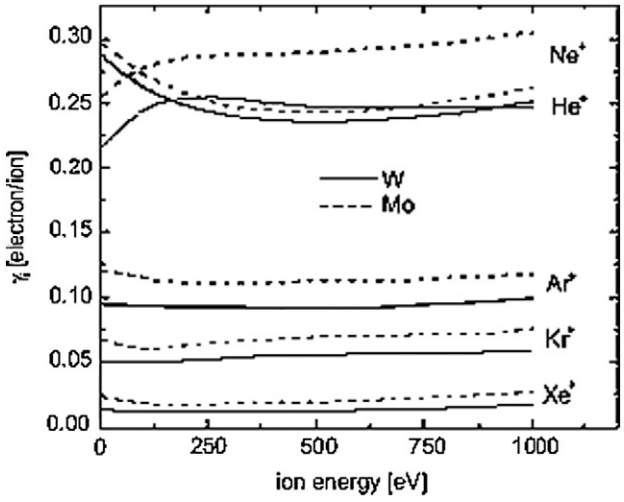

Fig. 4. The ion impact secondary electron emission yields, γ_{iee}, for rare gas ions incident at clean pure molybdenum and tungsten surfaces [66,67].

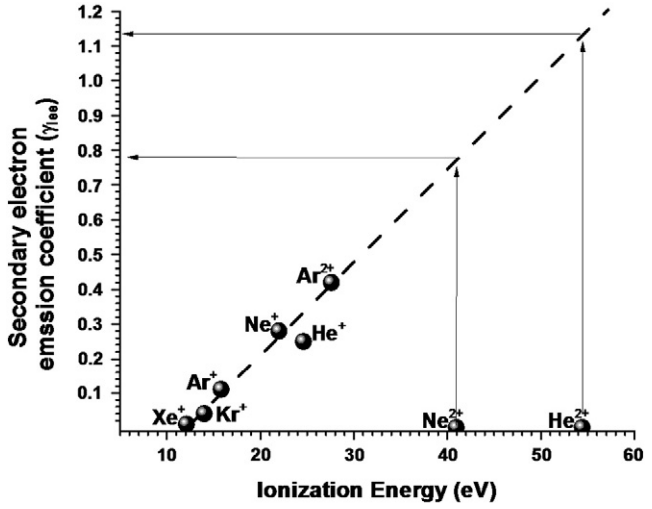

Fig. 5. The typical values of the secondary electron emission coefficient, γ_{iee}, for rare gas ions versus the ionization energy. The γ_{iee} values for doubly ionized neon and He have been extrapolated from the graph [69,72–74].

causing gas heating, atomic excitation and β ionization, or in the hollow cathode case, they can strike the opposing cathode surface. The cross section for atomic elastic interactions is similar to that of the argon ion and therefore, heating of the gas is one of the most probable and efficient energy-loss processes for the reflected atoms.

2.3.3. Electron emission mechanisms

2.3.3.1. Photoemission of electrons. If a photon with an energy hc/λ strikes a cathode surface and $hc/\lambda > eW_{Mat}$, where W_{Mat} is the work function of the material then an electron will be emitted from the surface [82]. For a given photon energy the emission rate of electrons is directly proportional to the intensity of the light and, above a threshold level of photon energy, the energy rather than the rate of emission of the electrons increases with increased photon energy [83,84]. Most metals have work functions in the range 2 to 6 eV and therefore de-excitation of the gas atoms normally used in hollow cathode discharges can cause emission of electrons [10].

2.3.3.2. Thermionic and field emission of electrons. As the temperature of the cathode surface increases, a small fraction of electrons have energies greater than the work function and can therefore be emitted. Moreover, quantum mechanics shows that electrons in the metal that approach the surface have a certain probability to "tunnel" through the surface barrier represented by the work function. These two phenomena are the basis of the thermal emission processes.

Field emission was first explained in the late 1920s as being quantum tunneling of electrons due to the presence of a large electric field and "Fowler–Nordheim equations" were developed to predict the field emission current. In addition to several important approximations, the equations require various assumptions in order to provide a reasonable description of the field emission process [33,48,85].

The existence of both high temperatures and large electric fields gives rise to a combined thermionic field-emission process which has been found to be considerably more important than a simple sum of the individual processes. The large enhancement due to the combined thermal field-emission yield compared to the two individual processes is demonstrated by the following examples from [29], see Table 2.

Table 2
Relative values of the electron emission current for thermal, field and thermal-field processes: the data is for a copper cathode ($W_{Cu} = 4.5$ eV).

Temp [K]	Electric field [V/m]	Thermal emission electron current, I_{TE} [A/m^2]	Field emission electron current, I_{FE} [A/m^2]	Combined emission electron current, $I_{T\text{-}FE}$ [A/m^2]	Increase, $\frac{I_{T-FE}}{(I_{TE})+(I_{FE})}$
2000	0	22		2×10^6	46,000
0	2×10^9		3.9		
5000	0	8.7×10^8	–	8×10^{11}	175
0	5×10^9	–	3.7×10^9		

2.4. Plasma structure of a normal glow discharge

Apart from the interactions between particles present in a plasma, the spatial variation of the concentration and energy of the different species within the discharge is of great importance. In the following, we will discuss the general structure of a simple parallel-plate DC plasma and then consider how this is modified in the hollow cathode geometry.

The distribution of electrical potential between the cathode and anode depends on many parameters, but an important characteristic is the Debye length, see Fig. 6. This is the distance over which significant variations of the charge density can spontaneously exist. We will see that, for example, low-voltage sheaths are typically a few Debye lengths wide [86]. The Debye length is [35]:

$$\lambda_D[\mathrm{cm}] = 743 \sqrt{\frac{T_e\ [\mathrm{eV}]}{n_e\ [\mathrm{cm}^{-3}]}}, \tag{11}$$

for which T_e is the electron temperature in eV and n_e is the plasma density in cm^{-3} [15,32,34,35,86]. Only the electron density and temperature are considered in the determination of the Debye length since it is their significantly greater mobility that is responsible for screening. It can be seen that λ_D decreases with increasing electron density and decreasing electron temperature and as such the Debye length describes the balance between the thermal and electrostatic energies of the ions and electrons. The electrostatic screening by the electron cloud that forms around an ion, or an applied electric potential, decreases by 1/e, 37%, over a distance of λ_D and at $3\lambda_D$ the potential is reduced to ~1%. For the plasmas considered in this study a typical value of $\lambda_D = 2 \times 10^{-2}$–$4 \times 10^{-4}$ cm for $n_e = 1 \times 10^9$–1×10^{13} cm^{-1} and $T_e = 1$–2.5 eV. For medium to low pressures 0.13 to ~1333 Pa (mTorr to ~10 Torr) discharges, λ_D is between 0.1 and 1% of the mean free path of the electrons. It is important to note that the Debye equation given above is only correct for $T_e \gg T_{ion}$ and $n_e \approx n_{ion}$; conditions which are not always the case for the entire discharge in a hollow cathode.

Fig. 6 from ref. [15] shows Debye length values as a function of the plasma density, n, versus the electron temperature, T_e, for several types of plasmas.

A schematic of the structure of a normal parallel-plate DC glow discharge is shown in Fig. 7 [87,88]. It is particularly instructive to correlate the luminosity of the different plasma regions with the electrical characteristics and the various particle collision events that occur in each region.

The potential applied between the cathode and the anode does not produce a uniform electric field between parallel-plate electrodes; the difference in the mobility of the electrons and ions produces a large electric field in front of the cathode, and to a lesser extent, close to the anode. These regions of the plasma are commonly referred to as the electrode sheaths. In spite of its importance, the cathode sheath is one of the most complicated and poorly understood parts of glow discharges [89]. As schematically shown in Fig. 7, the cathode sheath, which is the region connecting the bulk plasma to the cathode, contains three different regions [35], the ion sheath, the Debye sheath where the electron density rises but remains lower than the ion density, and the presheath, which consists of approximately equal densities of electrons and ions. The electrical potential in this last part is small and accelerates the

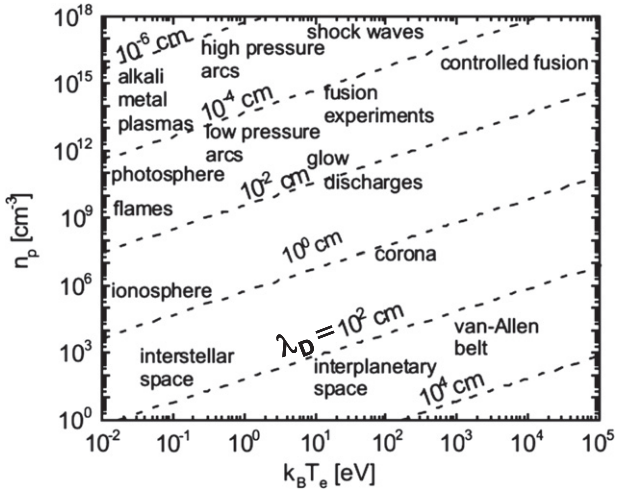

Fig. 6. Debye length values, λ_D (dashed lines), as a function of the plasma density, n, and electron temperature, T_e, for several types of plasmas [15].

ions present in the bulk plasma toward the sheath so that they achieve the Bohm velocity at the boundary between the presheath and sheath regions [15,34,35]. The Bohm velocity balances the component of velocity of the electrons along the direction of the electric field at the presheath/sheath boundary [37]. The thickness of the cathode sheath, l_s, depends on the characteristics of the plasma; high or low applied voltage, a collisionless sheath or with collisions (basically low or high pressure), the electron and ion temperatures, etc. [90]. A commonly used relation can be obtained by simultaneously solving the Child–Langmuir and Bohm equations [15,35,91,92]:

$$l_s = \frac{\varepsilon_o^{1/2} V_c^{3/4}}{\left(ekn_i^2 T_e\right)^{1/4}}. \tag{12}$$

Here, ε_o is the permittivity of free space, V_c is the cathode fall potential, e is the electron charge, k is the Boltzmann constant, n_i is the plasma ion density, and T_e is the electron temperature in eV. In general, the sheath thickness decreases as the ion density and electron temperature increase, and increases as the cathode-to-plasma potential increases. Various experimental studies of parallel-plate DC plasmas have shown that the sheath thickness decreases with increasing plasma current and the reciprocal of increasing pressure. For pressures from 5.3 to 27 Pa (0.04 to 2.0 Torr) the sheath thickness in a nitrogen plasma was seen to decrease as the reciprocal of the pressure and proportional to the reciprocal of applied voltage squared [93]. For RF plasmas, the sheath thickness varies approximately as $p^{-1/2}$ for pressures from 4 to 8 Pa (30–60 mTorr) and as the reciprocal of the pressure for values greater than 8–400 Pa (0.06–3.0 Torr) [15,35,94].

In general, it is recognized that the electric field (the ion and Debye sheaths together with the presheath) extends from the surface of the

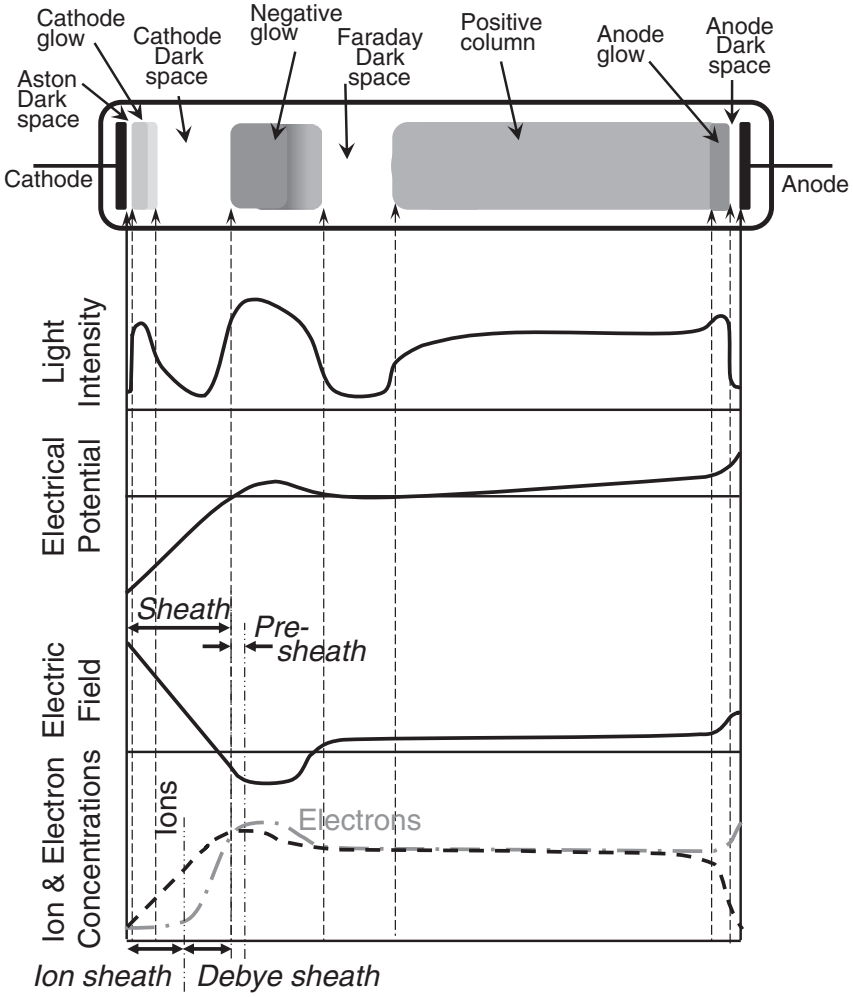

Fig. 7. A schematic illustration of the structure of a normal DC parallel-plate glow discharge.

cathode into the negative glow region. The total sheath thickness is often estimated to be five to eight times the Debye length.

The conventional description and explanation of the different regions shown in Fig. 7 are as follows:

- The Aston dark space is the first thin region in front of the cathode. The various electron emission processes which occur at the cathode surface cause this region to have a negative space charge and it is of low luminosity because the energy of the majority of the electrons is less than the Ar excitation energy, and is therefore also less than the ionization energy. This region is normally only observed for noble gas discharges [38].
- The neighbouring region is the cathode glow and is deemed to exist because here the electrons have gained enough energy (>11.55 eV) from the electric field to excite the neutral gas through collisions and, therefore, the region produces light of wavelengths that are characteristic of the gas, and also of atoms sputtered from the cathode surface [95–101].
- The subsequent cathode (Crooks or Hittorf) dark space is a darker region that has a strong electric field, a positive space charge, and a relatively high ion density. The length of this region depends on the gas pressure, the applied voltage, the plasma density, and the electron temperature. It is "dark" because as the electron energy increases to more than the 30 eV (the maximum of the excitation cross-section) the cross-section decreases, and therefore the luminosity decreases. The mobility of electrons is much higher than the mobility of ions; therefore, the predominant species in the dark space are ions, as shown in the schematic Fig. 7. For discharges operating at about 100 Pa (0.75 Torr), the length of the cathode dark space is typically less than a centimetre, but as mentioned earlier varies inversely, in a non-linear manner, with the gas pressure [23,33,35,36,102].
- The next region is the negative glow, which is often the brightest part of the entire discharge; it has a relatively abrupt boundary with the cathode dark space, but is more diffuse on the Faraday dark space side. The luminosity is greatest near the middle of the region and is caused by electrons that have energies close to 30 eV, such that the probability for excitation interactions is large. The electrons primarily lose energy by a series of both excitation and ionization interactions, as well as by elastic collisions, and this leads to dispersion in the distribution of their energy and produces a more gradual decrease in luminosity at the back edge of this region. Since the cross section for ionization is similar to that for excitation, the same high-energy electrons produce significant ionization of the gas atoms within the negative glow, as shown in Fig. 7. The collision processes that occur within this region produce a relatively high density of both negatively and positively charged particles and this is the first part of the plasma, in the direction from the cathode, where the positive and negative space charges are approximately equal. This means that the electric field is small in much of the negative glow volume. The electrons, due to their high mobility, primarily carry the electrical plasma current. At the end of the negative glow, the majority of the electrons have lost most of their energy. Therefore, the probability of excitation and ionization processes is low and consequently this is the beginning of the Faraday dark region [37].
- The Faraday dark space joins the negative glow with the positive column, the luminous region that connects to the anode.
- Typically, the positive column has a low net charge density and only a small electric field. This field is however, large enough to maintain sufficient excitation and ionization collisions with the gas atoms to permit electrical contact between the previous parts of the discharge and the anode and produce the observed luminosity. The high electric field near the electrodes means that the electrical impedance of those regions is larger than that of the positive column. Therefore, if at constant pressure, the length of the discharge tube is increased, the regions close to the cathode do not significantly change in size, but the positive column lengthens to form a longer uniform glow region [103]. Under certain conditions, the uniformity of the positive column can be perturbed with the formation of standing waves or moving luminous striations [33].
- The following region is the anode sheath region. The anode repels ions but attracts electrons from the positive column, this forms a region of negative space charge region and the acceleration of the electrons toward the anode produces the anode glow which is slightly brighter than the positive column. The visual appearance of the transition of the positive column to the anode glow region depends on the experimental conditions (the gas pressure and composition, the relative electrode sizes and the applied voltage), but often a dark or relative dark space can be seen [15,34,51]. This area is often referred to as the anode dark space [104]. Under some conditions, a narrow dark space may exist between the anode glow and the anode that is somewhat similar to the Aston's dark space at the cathode. Recent studies have shown that very close to the anode the density of electrons is strongly reduced and electron energy distribution becomes highly distorted and that this produces the observed abrupt decrease in the light emission [48,105–108].

In general, it is known that, for gas pressures from 0.001 to >10 Torr and applied voltages of a few hundred to a couple of thousand volts, the luminous and "dark" regions between the cathode and the Faraday dark space vary in position and length and can change in intensity and spectral content, but the changes as function of experimental parameters are smooth and continuous, as long as filamentary, or arc, breakdown does not occur. This continuity means that the same electron and ion interactions with the gas atoms are responsible for the different regions over this extensive parameter window. Additionally, it should be remembered that the light intensity generated in any region depends on the product of the density of gas atoms (this is constant for a given pressure and gas temperature), the number of electrons or ions with energies greater than the corresponding excitation threshold and the corresponding excitation cross-section.

The group of A. Bogaerts and others [37,95,109–113] reported that, based on an analysis of which Ar emission lines were emitted from the cathode glow and negative glow regions, the cathode glow luminosity was mainly caused by impact excitation collisions between the gas atoms and high energy argon ions and atoms (with these being produced by charge exchange), whereas the negative glow was generated by high energy electron-impact excitation.

Fig. 8 shows the Ar electron-impact excitation and ionization cross sections versus the electron energy. Here, it can be seen that a 50%

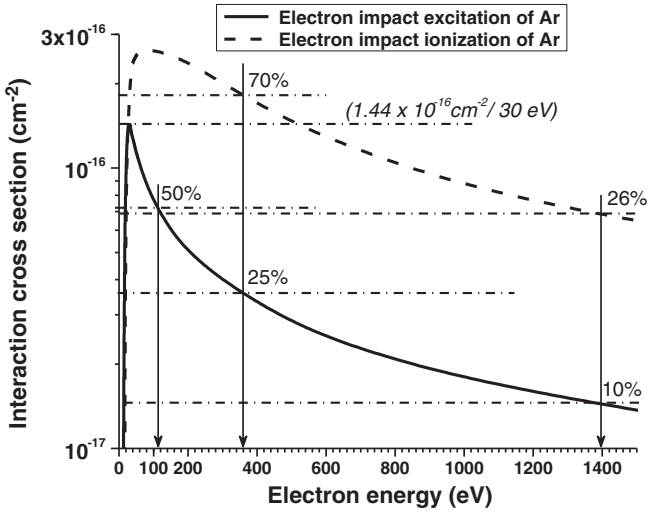

Fig. 8. Expanded view of Fig. 2 showing the electron impact excitation and ionization cross-sections for argon, together with the energies at which the excitation cross-section decreases to 50%, 25% and 10% of the maximum value [59,60].

decrease in the excitation cross section occurs when the electron energy is greater than about 110 eV (close to the maximum of the ionization cross section), a 75% decrease corresponds to electron energies of more than 340 eV and a 90% decrease to 1400 eV; the excitation maximum occurs at 30 eV [114]. It should be remembered that when an electron with an energy of, for example, 110 eV ionizes one or more gas atoms, then the energy of this primary electron is strongly reduced and the probability of excitation is therefore increased. Furthermore, the generated secondary electron would also be accelerated by the sheath and, on reaching ~25 eV would start to produce light. It is normally assumed that the maximum electron energy is proportional to the voltage applied to the discharge and that the minimum voltage to establish an inert gas parallel-plate discharge is 110–120 V [33,35]. Theoretical work by the A. Bogaerts group, of a 600–1200 V, 50–100 Pa (0.4–0.75 Torr) Ar DC discharge showed that, on average, the fraction of the maximum energy, according to the applied voltage, achieved by electrons and argon ions was 50% and 10–15%, respectively [109]. There is very little experimental data of the lack of luminosity of the cathode dark space, but the luminosity does not strongly change as a function of the applied voltage. Therefore:

> There is evidence that the luminosity of the cathode glow is mainly produced by high-energy ions and atoms.If the luminosity of the cathode glow is assumed to be due to electron impact this implies that the electron energy within the glow region is at least 30 eV. For the luminosity of the cathode dark space to be less than 25% of the cathode glow would require that the electrons have more than 340 eV, even though the applied voltage was 110–120 volts, which might be expected to give electron energies of 55–60 eV.Electron energies in excess of 340 eV would produce significant numbers of secondary electrons (and ions) within the cathode dark space, and these would (apart from perturb the sheath field) then be decelerated to energies where the probability of excitation interaction was high: light emission.

In conclusion, the available information strongly supports the idea that the cathode glow is produced primarily by collisions between high-energy ions and atoms with thermal-energy gas atoms and that the electron-impact excitation only starts to occur at the edge of the negative glow. Since most of the high-energy electrons start life at, or very close to, the cathode surface, the position where excitation first appears is fairly well defined (only elastic collisions with corresponding small energy losses occur below the excitation energy threshold) and this explains the relatively sharp front boundary of the negative glow. Therefore, from the cathode to the front edge of the negative glow, the energy of the majority of the electrons is less than ~25 eV, and very few ions are generated. Furthermore, over the distance from the edge of the negative glow to the beginning of the Faraday dark space, a significant number of electrons have energies greater than ~25 eV and this is where the majority of the gas-phase ionization events take place. This distance can be taken as a good estimate of the maximum trajectory for ionization and excitation of the electrons, emitted from the cathode and accelerated by the cathode sheath.

Fig. 3 shows that the cross section for the ion-impact excitation is large for ions with energies in excess of 100 eV. During such a collision, the ions lose a large amount of energy (15.7 eV) and this may be important for ion–cathode interactions. If most of the ions ended up with less than the excitation energy, then this could explain the existence of the Aston dark space, but of course, this does not agree with the fact that the ions sputter the cathode. An additional mechanism could be that the combination of all of the plasma–cathode interactions; ion bombardment, UV light absorption, high energy neutral atom bombardment, etc., results in the accumulation of a large amount of energy in the cathode surface (it is known that without cooling, the hollow cathode electrode can rapidly heat up to high temperatures, $T \gg 1000\ ^\circ C$) [115–117]. This input of energy should cause a corresponding local increase in the gas temperature and a localized reduction in the gas density that would in turn, reduce the number of ion–atom excitation collisions and, therefore, could explain the existence of the Aston dark space. Certainly various reports indicate that under some conditions this dark space is not observed; unfortunately insufficient details have been published to clarify the phenomena [33,90].

3. The conventional hollow cathode model

Although hollow cathode discharges have been used in applications such as spectroscopy for many years, it was not until the 1940s that an accepted theory for the hollow cathode effect was developed [13,30,33].

For experimental conditions of low power, or *p.d* less than the threshold value (approximately 0.1 Torr cm depending upon the gas being used), a normal non-resonant discharge in the hollow cathode (D-HC) is formed. For a planar, or linear, configuration the discharge in front of each facing cathode basically acts as independent discharges; each has a thin Aston dark space, a cathode glow layer, a cathode dark space and a negative glow region. For the cylindrical hollow cathode, the situation is equivalent in that there is a sheath and negative glow region in front of each part of the cathode. The centre core region between the cathodes, or at the centre of the cylinder, and the exit volume of the hollow space is occupied by the Faraday dark space and the rest of the discharge structure, the positive column, anode glow, etc. exists between the outlet of the cathode system and the anode, see Fig. 9.

As we have seen earlier, the high electric field region, or cathode sheath, extends from close to the cathode surface into the negative glow [48]. Additionally, for the particular case of the hollow cathode, the description of the sheath is complicated by the fact that many of the theoretical models assume a Maxwellian or Druyvesteyn electron energy distribution and, as we will see later, this is not correct for typical operating conditions [23,118].

The fact that electrons can only escape from the plasma, or travel to the anode, by moving along the axis of the hollow cathode means that even though the electron generation processes are the same as for a planar discharge (mainly, gas phase ionization in the negative glow and ion impact induced secondary electron emission from the cathode), the loss rate of electrons is low and, therefore the plasma density is high [48]. Most plasma studies have shown that the electron temperature of hollow cathode discharges is similar to that obtained in a common planar system; however, the increased plasma density means that the cathode sheath is thinner than for planar electrodes [33].

As the experimental conditions are changed (larger applied voltage or a change in *p.d* so that it is between the minimum and maximum values for the establishment of the quasi-resonant hollow cathode discharge, HCD), the negative glow region expands until the central Faraday dark space region disappears. Coincidentally with this expansion, there is an increase in the brightness of the discharge, a significant increase in the plasma density and often an exponential increase in the plasma current to values that can be several orders of magnitude

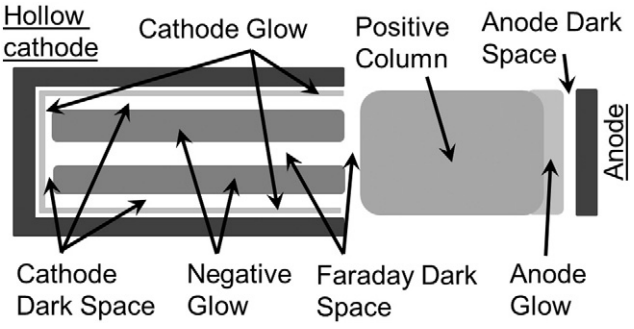

Fig. 9. A schematic representation of a plasma in a DC hollow cathode before the establishment of the quasi-resonant HCD state.

greater than that found for the D-HC [13,119,120]. This discharge is the true quasi-resonant HCD. The change from D-HC to HCD with increased applied voltage (power) is due to the increase in the cathode sheath that in turn produces an increase in the average electron energy and therefore an expansion of the width of the negative glow region. Similarly, for a given pressure, a reduction in the separation of the cathode surfaces can also produce the overlap of the opposing negative glow regions. For a given voltage and cathode separation, the thickness of the various discharge layers is dependent on the gas pressure and type [37,121]. If the pressure is increased, the cathode dark space and sheath become thinner and the resulting increase in the number of gas phase collisions means that the negative glow region also becomes thinner. Conversely, if the gas pressure is strongly decreased, the cathode dark space and sheath become larger and even though the thickness of the negative glow does increase slightly, the majority of the space between the sides of the cathode becomes occupied by the cathode dark space. Unfortunately, the conventional HCD models do not clearly explain why the low gas pressure condition does not produce the HCD state [122–124].

The configuration of a thin sheath in front of each part of the cathode surface and a bright combined negative glow region which fills the majority of the volume of the hollow cathode results in the formation of a potential well in the central region which is close to the anode potential [15,125]. This plasma structure is thought to promote an oscillatory motion of electrons between the opposing cathode sheath regions, the Pendel effect or pendulum trapping of the electrons [13,30,31,124,126,127]. The resulting increase in the electron trajectory is deemed to cause a large increase in the number of ionization events.

Most models of the hollow cathode effect conclude that there are two groups of electrons, a low-energy population whose velocity distribution is Maxwellian and uniform throughout most of the negative glow, and a high-energy group generated from the bombardment of, and photoemission from, the cathode surface, as well as gas-phase ionization events caused by ion-impact collisions close to the cathode surface [37,50,121,128,129]. The low-energy group is a combination of the elastic-collision thermalized high-energy electrons and those electrons produced by gas-phase ionization of the neutral gas atoms by high-energy electrons within the central negative glow region. Therefore, the density of low-energy electrons is several orders of magnitude greater than that of high-energy ones; moreover, the energy of the low-energy electrons is such that they do not cause ionization and produce more plasma electrons. Additionally, the low field in the negative glow region means that this group of electrons is not accelerated to higher energies. However, the group of high-energy electrons is accelerated by the cathode sheath potential (see ref. [99]) and penetrates the negative glow region with high energy.

The conventional models consider that the mean free path of the high-energy electrons is sufficiently large that they are able to pass through the negative glow region, while causing a few ionization events, reach the opposing cathode sheath and be reflected back through the central region, causing additional ionization events during each pass (the pendulum effect) [30,118,130]. Several authors have estimated the number of oscillations of the high-energy electrons and values from 1 to more than 3 have been reported [31,118,130]. The pendulum motion of the electrons means that their kinetic energy, and therefore their velocity and interaction cross section, oscillates between a maximum in the centre of the discharge to minimum values close to each opposing surface of the cathode. As we have seen, elastic collisions of the electrons with other particles produce only small reductions in the electron energy; the elastic interaction cross-section is larger than the ionization or excitation cross-sections. Elastic collisions can cause a large change in the momentum of the electron with approximately a sixth (depending on the geometry of the cathode) of the electrons leaving the discharge through the hollow cathode end aperture.

Many conventional models of hollow cathode discharges consider that; (a) the pendulum electrons participate in ionization reactions in the sheath close to the cathode and in this way generate secondary electrons which can be accelerated to high energy [131], and (b) there is enhanced electron emission from the cathode due to bombardment by photons and metastable atoms [23,31,118,132–134].

Studies by Sturges and Oskam concluded that the role of metastable species was not important for the hollow cathode effect in hydrogen and noble gases [135,136]. However, in contrast to various other papers, the same study concluded that there was little difference between the hollow cathode discharge in hydrogen and argon. The details of the cathode geometry, the gas type and gas pressures used in the two papers show that the majority of the plasmas studied were probably the D-HC rather than a true hollow cathode discharge, HCD, and therefore the importance of metastable atoms for the formation of the quasi-resonant hollow cathode condition has not been clearly determined.

In general, the conventional models in use today affirm that the hollow cathode discharge condition exists because the “pendulum” oscillatory trajectory of the high-energy electrons produces increased ionization of the neutral gas that, in turn, results in the formation of a high plasma density, high luminosity, and large discharge current. Additionally, the enhanced electron emission due to the increased number of photons and metastable neutrals can provide, under some conditions, an important contribution to the plasma density.

One of the major problems for any phenomenological model of the high density HCD is the explanation of how small increases in the applied voltage can provide a super-linear increase in the discharge current and light production.

As we have seen, electrons can be generated in the gas phase by an electron colliding with either a neutral, an excited atom or an ion, and since all the cross sections are large for electron energies between ~20 and 1000 eV, the ionization probability is greatest in the central region of the discharge where the electrons have the highest kinetic energy. The similarity of the excitation and ionization cross sections means that the central region also produces most of the light [119,120,137]. For the ionization of neutral argon atoms, each collision reduces the electron energy by at least 15.67 eV [35]. The generated secondary electrons have energies of only a few eV and therefore do not contribute to the production of additional electrons or ions, or to the excitation of atoms; furthermore, they remain within the central region of the cathode since they are repelled by the electric fields of the pre-sheath and sheath. A number of authors [23,138–141] have proposed that the high-energy pendulum electrons cause ionization within the sheath such that the generated secondary electrons are accelerated by the cathode sheath to sufficiently high energies to cause additional ionization events. This idea has often been the basis of the superlinear relation between the production of electrons and the applied voltage, which is required to explain the very large currents observed for the HCD state. Unfortunately, there are several problems with this proposal. Firstly, the energy of electrons bouncing from one sheath to the opposing one changes as a pendulum, from having the highest kinetic energy in the central region to having the highest potential energy and zero velocity at the extreme of the trajectory within the sheath. In electron collisions, potential energy is not useful for producing ionization. Secondly, as we have seen, wherever there is ionization, light emission due to excitation also occurs. However, changes in the luminosity of the sheaths of hollow cathode discharges have not been reported for the transition from the D-HC to the HCD state [21,33,36,137,142–144].

Other electron production processes involve the impingement of ions, high-energy neutrals, and excited atoms on the cathode. As noted earlier, the number of secondary electrons produced by photoemission, thermionic and field emission, and impact with high-energy species only increases slightly with increasing energy of the bombarding species, provided that the energy is greater than the threshold value for the process. The electrons generated by these processes appear within the strong sheath electric field and therefore are rapidly accelerated toward the centre of the discharge and can cause additional gas-phase ionization. Obviously, the number of secondary

electrons does depend on the number of collisions and therefore the plasma density, but the relations are linear, not super-linear.

It was proposed that if the mean free path of the electrons is greater than the diameter of the cathode, the electrons might collide with the opposing side of the cathode. However, it should be noted that the largest interaction cross section for electrons is for elastic collisions between electrons and neutral atoms, and although the electron loses only a small amount of its energy, this is more than sufficient to prevent the electron reaching the opposing cathode, even without the extreme electrostatic repulsion involved in such an impact. Additionally, an excessively large electron mean free path (a large number of pendulum oscillations) would mean that there must be few ionization events during each pass through the central region. Conversely, a very small mean free path would not allow the pendulum motion to occur [24,145–151].

The other gas-phase ionization processes are the ion-impact ionization of a neutral or excited atom and since these cross sections increase with energy, they would be expected to occur mainly in the sheath close to the cathode. Electrons generated in this zone are accelerated by the sheath and can participate in additional ionization processes. However, the ion-impact cross section is about an order of magnitude lower than electron-impact interactions except for ions close to 1 keV. The ion–atom excitation cross section is also similar to that for ionization. Therefore, if ion-impact processes were very significant for the hollow cathode condition, then a distinctively bright area in the sheath close to the cathode should observed. Few such measurements have been reported. The photographs shown in [120], for high pressure discharges, where the probability of ion–atom collisions is high, do appear to show such a bright zone. Other articles also show luminosity in this region and indicate that gas phase ion impact ionization is a process that can contribute to the production of electrons [137,144]. However, the sum of the above processes, including any oscillatory trajectory of the electrons, cannot explain the observed very large increase in current for small increases in voltage when the discharge is in the HCD state. All of the processes only describe linear or sub-linear increases in the plasma density as the sheath field is increased. Therefore, we conclude that none of the above schemes are sufficient to fully explain the existence of the HCD state.

3.1. New considerations

A large number of authors have published descriptions of the hollow cathode effect and theoretical models of the HCD, but very few have considered what happens as a normal discharge, established at a low voltage, changes into the much denser HCD state [137,144]. Several groups have published descriptions of the radial distribution of the metastable atoms, ions, electric field, and light intensity across the hollow cathode [1,65,137,143,144,146,152]. In some of these references [144], for example, the radial variation of the luminosity of the plasma was recorded as a function of the plasma current and the gas pressure for conditions corresponding to a normal discharge (labelled as AGD mode in the reference and Fig. 10 below) and the HCD condition (labelled as the HCE mode). We use these results to help describe our new model of the HCD effect.

In Fig. 11, it can be seen that for the D-HC condition – that is, for voltages and currents less than 340 and 25 mA, respectively – there are two negative glow regions producing light approximately 1–2 mm from the surface of the hollow cathode. For currents between 30 to 70 mA, values that correspond to the quasi-resonant HCD condition, the intensity of the emitted light increases and the light distribution is almost uniform across the central region of the hollow cathode beginning at ~1 mm from the surface. At the highest voltages, there is a small broad peak at the centre of the discharge. It should be noted that the distance from the cathode to the edge of the bright area advances very little once the HCD condition has been established, demonstrating that the width of the cathode sheath changes very little even though the current

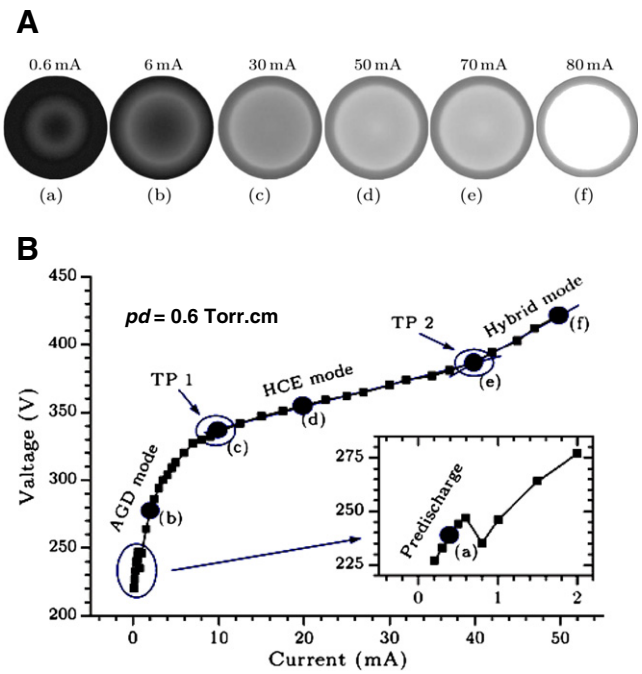

Fig. 10. Current/voltage characteristic, and plasma images as a function of current in an Ar hollow cathode discharge operating, at $p.d = 1.5$ Torr cm.

increases from 30 to 80 mA. Narrow peaks of light emission can be seen very close to each side of the cathode surface and these are probably from ion-impact excitation of the gas (cathode glow). These peaks exist for the lowest currents, 6 mA, up to the highest values studied and their form and position is relatively constant. The total light emission intensity of the discharge increases as the current increases. The following conclusions can be obtained from these results:

- Since the ion-impact excitation peak changes little from the D-HC to the HCD state, then this ionization process is probably not one of the fundamental causes of the quasi-resonant HCD condition.
- From the photographs in Figs. 10 and 11, we see that for the D-HC condition, the discharge negative glow region extends from about 1 to 2.5 mm in front of the hollow cathode surface. This means that from 0 to 1 mm and 2.5 to 5 mm (the centre of the cathode), the majority of the electrons have less than ~25 eV (an energy for which the excitation cross section is sufficiently large to result in a notable emission of light).
- As the voltage is increased, the front edge of the negative glow moves closer to the cathode, ~0.8 mm, and the far edge of this region expands toward the centre of the cathode.

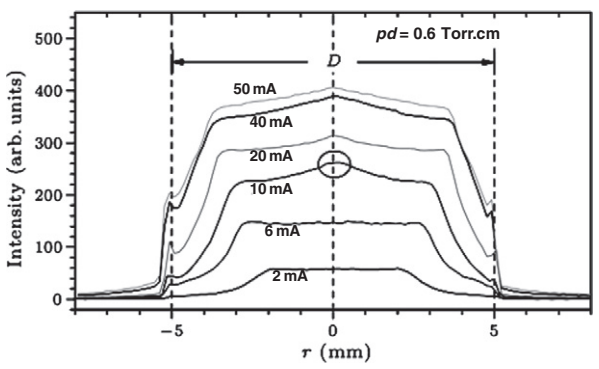

Fig. 11. Radial profiles of the light intensity as a function of the discharge current in an Ar hollow cathode operated at $p.d = 1.5$ Torr cm.

- At the voltage corresponding to the transition from D-HC to HCD, the edge of the negative glow region slightly passes the centre of the cathode and this produces the broad luminescent peak because of the overlapping "negative glow" regions.
- Once the HCD state has been established, the voltage need only be increased from 360 to 380 V (5.5%) to cause the current to increase from 30 to 70 mA (230%). This implies that a 5.5% increase in the energy of the electrons more than doubles the number of electrons.

Fig. 12 shows schematically what happens during the transition from the D-HC state to the HCD state. The space between the front-edge and back-edges of the negative glow corresponds to the distances from the cathode over which a significant number of the electrons have energies greater than the excitation threshold; we refer to this as the excitation/ionization trajectory. Closer to the cathode surface and the centre of the cylinder, less light is produced; therefore, the energy of the majority of the electrons is less than the excitation threshold. As the applied voltage V_{appl} is increased, the excitation/ionization trajectory increases until the trajectories from different parts of the cathode surface overlap. The centre region of the cathode then has a somewhat greater luminosity and, as seen in ref. [144], this condition corresponds to the start of the HCD state [33].

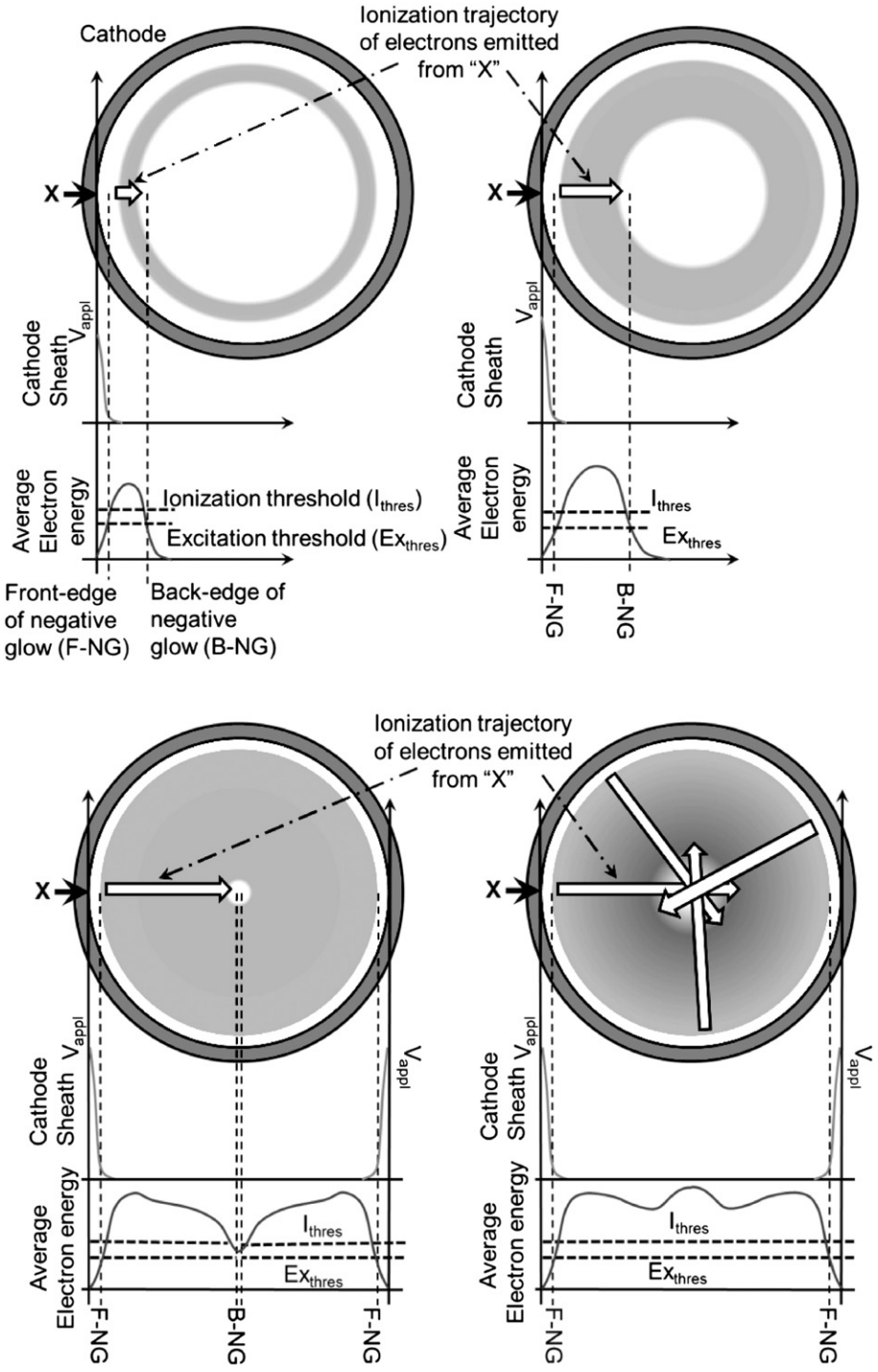

Fig. 12. A schematic representation of the plasma structure during the transition from the D-HC to HCD condition, i.e. as the voltage is increased for a constant gas pressure and system geometry.

Here, we consider the D-HC to HCD transition as a consequence of the increase in the applied voltage. However, it is clear that a similar process occurs if the distance across the hollow cathode is decreased. Obviously, if the applied voltage is not changed, the excitation/ionization trajectory is constant, but when the critical cathode diameter is reached, the back-edges of the two negative glow regions overlap in a manner similar to that described above. If the pressure, cathode diameter, and applied voltage are such that the HCD condition has been established, then an increase in the gas pressure will cause a reduction in the excitation/ionization trajectory because of an increased number of collisions and this would cause a change from HCD to D-HC. It has been reported that for larger cathode diameters, a higher voltage is required to establish the HCD condition and that with a constant applied voltage, the current density decreases as the pressure is increased [153,154].

As mentioned in point 5 above and as reported by many groups, in the HCD state only a relatively small increase in voltage is needed to produce a very large increase in current and a corresponding increase in the luminosity [1,140,143,155,156]. The problem is that such a small voltage increase can only cause a small increase in the excitation/ionization trajectory and therefore only a very small proportion of additional electrons can reach the opposite cathode sheath and this, together with the points described above, imply that the oscillating pendulum motion of the electrons does not occur. An increase of the electron energy by approximately 20 eV (see above applied voltage change of 360 to 380 V), in the HCD state, corresponds to only one additional ionization event and obviously this is not enough to explain the large increase in the discharge current.

3.2. A proposed explanation

The plasma density, and therefore the discharge current, depends on the establishment of a balance between the generation and loss of electrons (we assume that there is a general net balance between the number of electrons and ions). It is reasonable to assume that the disappearance rate of electrons (loss to earth, recombination, and arrival at the anode) is approximately proportional to the plasma density. Therefore, during the transition from the D-HC to the HCD state, an additional efficient electron generation mechanism begins to dominate. As we have discussed earlier, the principal electron production mechanisms are as follows:

In the negative glow:

$$e^- + \mathrm{Ar} \rightarrow \mathrm{Ar}^+ + 2e^- \quad (13)$$

$$e^- + \mathrm{Ar}^* \rightarrow \mathrm{Ar}^+ + 2e^- \quad (14)$$

$$e^- + \mathrm{Ar}^+ \rightarrow \mathrm{Ar}^{2+} + 2e^- . \quad (15)$$

At, or close to, the cathode surface:

$$\mathrm{Ar}^+ + \mathrm{Cathode} \rightarrow \mathrm{Ar} + e^- \quad (16)$$

$$\mathrm{Ar}^{2+} + \mathrm{Cathode} \rightarrow \mathrm{Ar} + e^- \quad (17)$$

$$\mathrm{Ar}^* + \mathrm{Ar}^* \rightarrow \mathrm{Ar}^+ + \mathrm{Ar} + e^- \quad (18)$$

$$\mathrm{Ar}^+ + \mathrm{Ar} \rightarrow 2\mathrm{Ar}^+ + e^- \quad (19)$$

$$\mathrm{Ar}^+ + \mathrm{Ar}^* \rightarrow 2\mathrm{Ar}^+ + e^- . \quad (20)$$

The secondary electron emission coefficients for Ar^+ and Ar^{2+} ions with energies less than 1 keV are, depending on the target material, typically in the range of 0.12 and 0.45, respectively [69,72–76].

Obviously, the importance of each of these mechanisms depends on a combination of the interaction cross section, the density of the energetic species (electrons or ions) and the density of the target species. The plasma density of the HCD state depends on the experimental parameters but, as mentioned in the introduction, typical values are from 10^{11} to more than 10^{13} cm^{-3} [18,19], and this is often two orders of magnitude more than the D-HC condition [3,22]. Neutral Ar is the most numerous species and there will be much smaller quantities of Ar* and Ar^+. As explained earlier, reactions described by Eqs. (18)–(20) occur close to the cathode surface and ions are rapidly lost to the cathode. The first three gas-phase reactions, Eqs. (13)–(15), produce ions within the negative glow where there is little or no electric field. Under the HCD condition, the negative glow region of the discharge is also the collection point for electrons produced on, or close to, the cathode surface. This combination of relatively high ion concentration and large flux of high-energy electrons provides the correct conditions for the production of doubly-ionized argon ions [157,158].

Having a high density of electrons with sufficient energy to cause the second ionization process is not sufficient; the singly-charged ions must be confined within the plasma region where the second ionization can take place (see page 24 in [159]). The most important parameter is $n_e\tau_i$, the product of the plasma electron density n_e and the ion confinement time τ_i. This product is largest in the central region of the hollow cathode discharge [159].

Several groups have reported the presence of Ar^{2+} and the increased generation of such ions in the HCD state [160–166]. The importance of these ions is, firstly, that they are accelerated to higher energies by the cathode sheath, and secondly, when they strike the cathode, they generate approximately four times the number of electrons than singly-charged ions [67,72]. These additional electrons, in turn, generate more ions, including more doubly-charged ions, in a quasi-resonant manner that greatly increases the plasma density and explains the observed large increase in the plasma current.

Therefore, we conclude that the “hollow cathode effect” is not dominated by pendulum electrons, but depends on the quasi-resonant generation of doubly-charged gas ions within the central negative glow region of the discharge.

An obvious implication of the present model is that the HCD state is not possible in a hydrogen discharge since no doubly-charged hydrogen ion exists. An extensive review of the published work on hydrogen discharges in a hollow cathode [167–171] shows that many studies have involved high-density discharges in a D-HC hollow cathode, but we have not found any report that unmistakably demonstrates the existence of a quasi-resonant HCD state using pure hydrogen.

3.3. Experimental tests

As an additional verification we performed a series of experiments in our 0.8 cm diameter, 4.5 cm long, water-cooled cylindrical hollow cathode [172,173]. We measured the I–V characteristics of a DC discharge as a function of gas pressure and gas flow using 99.99% pure argon, helium and hydrogen. The vacuum chamber was stainless steel evacuated using a turbomolecular pump with a two-stage mechanical pumping system which provided a background pressure of $<1.33 \times 10^{-4}$ Pa ($<10^{-6}$ Torr). Fig. 13a, b and c shows the I–V curves for argon, helium and hydrogen plasmas, respectively, using gas pressures from 40 to 347 Pa (0.3 to 2.6 Torr) and for gas flows of 10, 50 and 100 sccm. The same scales have been used for all graphs to facilitate data comparison. For argon, pressures below 53 Pa (0.4 Torr, $p.d =$ 0.32 Torr cm) did not produce the quasi-resonant HCD state. However, the HCD condition was clearly established at pressures >53 Pa (>0.4 Torr), but there was no noteworthy dependence of the I–V characteristics on the gas flows from 10 to 100 sccm. The HCD state was established at all helium gas pressures, 40 to 347 Pa (0.3 to 2.6 Torr), and gas flows, 10 to 100 sccm. However, using hydrogen, there was little difference in the I–V characteristics from 67 to 312 Pa (0.5 to 2.34 Torr) and the HCD state was not obtained. Higher gas pressures and higher

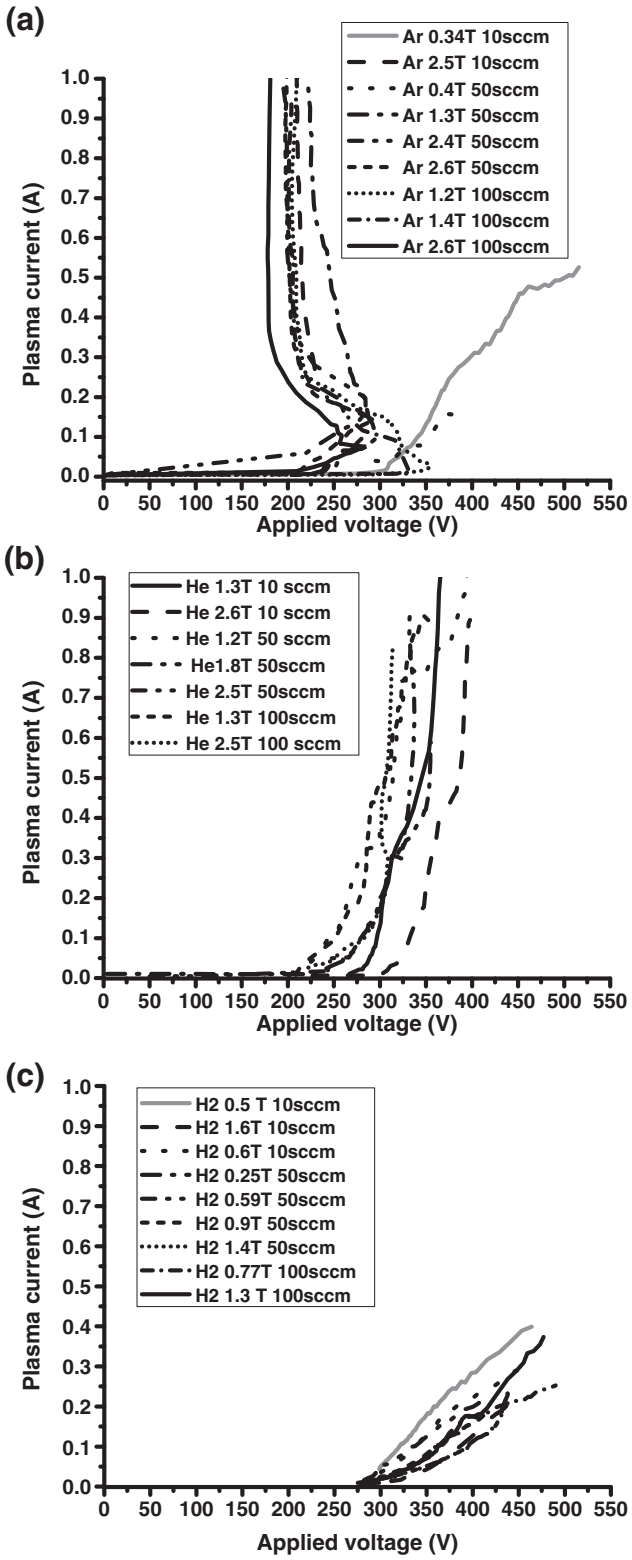

Fig. 13. Measured I–V characteristics for a 0.8 cm-diameter, 4.5 cm long, water-cooled hollow cathode operated at pressures and gas flow rates shown in the insets, a) argon, b) helium and c) hydrogen.

voltages resulted in filamentary arcing between the hollow cathode and the vacuum chamber, but even at 400 Pa (3.0 Torr) and 450 V, there was no evidence of the existence of the high-current HCD condition.

Fig. 14 shows the I–V data for argon, helium and hydrogen discharges using a gas flow of 50 sccm and gas pressures close to 173 Pa

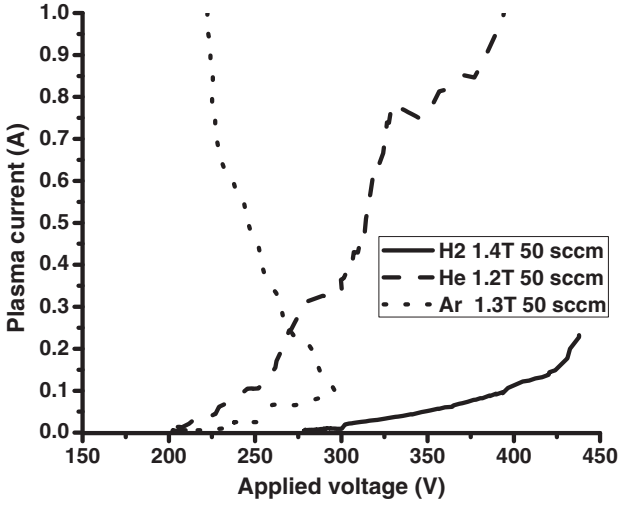

Fig. 14. A comparison of the I–V characteristics of argon, helium and hydrogen DC discharges in a 0.8 cm-diameter, 4.5 cm long, water-cooled hollow cathode operated at a gas flow of 50 sccm and pressure of 173 ± 13 Pa (1.3 ± 0.1 Torr).

(1.3 Torr). The HCD state was observed for argon and helium, but not for hydrogen. The I–V characteristics for argon and helium show that for a plasma current of 0.5 A, the average plasma voltage is ~210 and ~310 V, respectively. The difference is related to the fact that the second ionization energy of helium is considerably higher than that for argon and therefore fewer doubly-charged helium ions are formed.

4. Hollow cathode arc

If excessive electrical power is applied to a hollow cathode system, the energy deposited in the cathode causes it to reach high temperatures [115,116,119,174,175]. Obviously, the plasma power versus cathode temperature increase depends very much on the degree of cooling, the electrode geometry, gas type, and pressure. If the temperature reaches more than 1000 °C, thermal-field emission of electrons from the cathode starts to become an important additional source of electrons [176]. Under such conditions, the plasma density can become greater than 10^{13} cm^{-3} and, as shown in Fig. 1, the plasma current can increase to values considerably larger than those found in the HCD condition.

The HCA mode is typically characterized by voltages less than 100 V and currents of several amperes, depending on the cathode surface area. Obviously, such high cathode temperatures also increase the gas temperature and this can enhance rarefaction near the cathode and produce important modifications to the plasma properties, gas-phase chemical reactions can cause significant heating of the substrates during thin film deposition [27,29]. The transition from HCD to HCA occurs rapidly when a threshold current density is reached and the new electron emission process become operative. The additional electrons can attain relatively high energies since they are accelerated by the complete sheath before they reach the negative glow region. However, the decrease in the applied voltage caused by the change in the plasma impedance considerably reduces the sheath field and therefore the maximum electron energy. This in turn can be expected to reduce the generation of the doubly-charged ions in the negative glow.

5. Geometric aspects

As mentioned earlier in this review, studies have shown that there are conditions under which the HCD state can and cannot be established. In general, research groups have observed that for values of the product of the pressure p and the diameter of the cathode d between approximately 0.1 and 37 Torr cm, the HCD mode can be

Table 3
The darker shaded area (13.56 MHz RF) and the lighter shaded area (a 200 ns negative DC pulse) correspond to times for which the electron energy (electron velocity) is sufficiently large for an electron to perform three oscillations across the diameter of a hollow cathode discharge; as required for the pendulum theory.

Electron energy (eV)	Time [s] for three sheath–to–sheath electron oscillations																	
	Cathode diameter (m)																	
	0.01	0.02	0.03	0.04	0.05	0.06	0.07	0.08	0.09	0.1	0.15	0.2	0.25	0.3	0.35	0.4	0.45	0.5
1	5.1E–08	1.0E–07	1.5E–07	2.0E–07	2.5E–07	3.0E–07	3.5E–07	4.0E–07	4.6E–07	5.1E–07	7.6E–07	1.0E–06	1.3E–06	1.5E–06	1.8E–06	2.0E–06	2.3E–06	2.5E–06
2	3.6E–08	7.2E–08	1.1E–07	1.4E–07	1.8E–07	2.1E–07	2.5E–07	2.9E–07	3.2E–07	3.6E–07	5.4E–07	7.2E–07	8.9E–07	1.1E–06	1.3E–06	1.4E–06	1.6E–06	1.8E–06
3	2.9E–08	5.8E–08	8.8E–08	1.2E–07	1.5E–07	1.8E–07	2.0E–07	2.3E–07	2.6E–07	2.9E–07	4.4E–07	5.8E–07	7.3E–07	8.8E–07	1.0E–06	1.2E–06	1.3E–06	1.5E–06
4	2.5E–08	5.1E–08	7.6E–08	1.0E–07	1.3E–07	1.5E–07	1.8E–07	2.0E–07	2.3E–07	2.5E–07	3.8E–07	5.1E–07	6.3E–07	7.6E–07	8.9E–07	1.0E–06	1.1E–06	1.3E–06
5	2.3E–08	4.5E–08	6.8E–08	9.1E–08	1.1E–07	1.4E–07	1.6E–07	1.8E–07	2.0E–07	2.3E–07	3.4E–07	4.5E–07	5.7E–07	6.8E–07	7.9E–07	9.1E–07	1.0E–06	1.1E–06
6	2.1E–08	4.1E–08	6.2E–08	8.3E–08	1.0E–07	1.2E–07	1.4E–07	1.7E–07	1.9E–07	2.1E–07	3.1E–07	4.1E–07	5.2E–07	6.2E–07	7.2E–07	8.3E–07	9.3E–07	1.0E–06
7	1.9E–08	3.8E–08	5.7E–08	7.7E–08	9.6E–08	1.1E–07	1.3E–07	1.5E–07	1.7E–07	1.9E–07	2.9E–07	3.8E–07	4.8E–07	5.7E–07	6.7E–07	7.7E–07	8.6E–07	9.6E–07
8	1.8E–08	3.6E–08	5.4E–08	7.2E–08	8.9E–08	1.1E–07	1.3E–07	1.4E–07	1.6E–07	1.8E–07	2.7E–07	3.6E–07	4.5E–07	5.4E–07	6.3E–07	7.2E–07	8.1E–07	8.9E–07
9	1.7E–08	3.4E–08	5.1E–08	6.7E–08	8.4E–08	1.0E–07	1.2E–07	1.3E–07	1.5E–07	1.7E–07	2.5E–07	3.4E–07	4.2E–07	5.1E–07	5.9E–07	6.7E–07	7.6E–07	8.4E–07
10	1.6E–08	3.2E–08	4.8E–08	6.4E–08	8.0E–08	9.6E–08	1.1E–07	1.3E–07	1.4E–07	1.6E–07	2.4E–07	3.2E–07	4.0E–07	4.8E–07	5.6E–07	6.4E–07	7.2E–07	8.0E–07
20	1.1E–08	2.3E–08	3.4E–08	4.5E–08	5.7E–08	6.8E–08	7.9E–08	9.1E–08	1.0E–07	1.1E–07	1.7E–07	2.3E–07	2.8E–07	3.4E–07	4.0E–07	4.5E–07	5.1E–07	5.7E–07
30	9.2E–09	1.8E–08	2.8E–08	3.7E–08	4.6E–08	5.5E–08	6.5E–08	7.4E–08	8.3E–08	9.2E–08	1.4E–07	1.8E–07	2.3E–07	2.8E–07	3.2E–07	3.7E–07	4.2E–07	4.6E–07
40	8.0E–09	1.6E–08	2.4E–08	3.2E–08	4.0E–08	4.8E–08	5.6E–08	6.4E–08	7.2E–08	8.0E–08	1.2E–07	1.6E–07	2.0E–07	2.4E–07	2.8E–07	3.2E–07	3.6E–07	4.0E–07
50	7.2E–09	1.4E–08	2.1E–08	2.9E–08	3.6E–08	4.3E–08	5.0E–08	5.7E–08	6.4E–08	7.2E–08	1.1E–07	1.4E–07	1.8E–07	2.1E–07	2.5E–07	2.9E–07	3.2E–07	3.6E–07
60	6.5E–09	1.3E–08	2.0E–08	2.6E–08	3.3E–08	3.9E–08	4.6E–08	5.2E–08	5.9E–08	6.5E–08	9.8E–08	1.3E–07	1.6E–07	2.0E–07	2.3E–07	2.6E–07	2.9E–07	3.3E–07
70	6.1E–09	1.2E–08	1.8E–08	2.4E–08	3.0E–08	3.6E–08	4.2E–08	4.8E–08	5.4E–08	6.1E–08	9.1E–08	1.2E–07	1.5E–07	1.8E–07	2.1E–07	2.4E–07	2.7E–07	3.0E–07
80	5.7E–09	1.1E–08	1.7E–08	2.3E–08	2.8E–08	3.4E–08	4.0E–08	4.5E–08	5.1E–08	5.7E–08	8.5E–08	1.1E–07	1.4E–07	1.7E–07	2.0E–07	2.3E–07	2.5E–07	2.8E–07
90	5.3E–09	1.1E–08	1.6E–08	2.1E–08	2.7E–08	3.2E–08	3.7E–08	4.3E–08	4.8E–08	5.3E–08	8.0E–08	1.1E–07	1.3E–07	1.6E–07	1.9E–07	2.1E–07	2.4E–07	2.7E–07
100	5.1E–09	1.0E–08	1.5E–08	2.0E–08	2.5E–08	3.0E–08	3.5E–08	4.0E–08	4.6E–08	5.1E–08	7.6E–08	1.0E–07	1.3E–07	1.5E–07	1.8E–07	2.0E–07	2.3E–07	2.5E–07
200	3.6E–09	7.2E–09	1.1E–08	1.4E–08	1.8E–08	2.1E–08	2.5E–08	2.9E–08	3.2E–08	3.6E–08	5.4E–08	7.2E–08	8.9E–08	1.1E–07	1.3E–07	1.4E–07	1.6E–07	1.8E–07
300	2.9E–09	5.8E–09	8.8E–09	1.2E–08	1.5E–08	1.8E–08	2.0E–08	2.3E–08	2.6E–08	2.9E–08	4.4E–08	5.8E–08	7.3E–08	8.8E–08	1.0E–07	1.2E–07	1.3E–07	1.5E–07
400	2.5E–09	5.1E–09	7.6E–09	1.0E–08	1.3E–08	1.5E–08	1.8E–08	2.0E–08	2.3E–08	2.5E–08	3.8E–08	5.1E–08	6.3E–08	7.6E–08	8.9E–08	1.0E–07	1.1E–07	1.3E–07
500	2.3E–09	4.5E–09	6.8E–09	9.1E–09	1.1E–08	1.4E–08	1.6E–08	1.8E–08	2.0E–08	2.3E–08	3.4E–08	4.5E–08	5.7E–08	6.8E–08	7.9E–08	9.1E–08	1.0E–07	1.1E–07
600	2.1E–09	4.1E–09	6.2E–09	8.3E–09	1.0E–08	1.2E–08	1.4E–08	1.7E–08	1.9E–08	2.1E–08	3.1E–08	4.1E–08	5.2E–08	6.2E–08	7.2E–08	8.3E–08	9.3E–08	1.0E–07
700	1.9E–09	3.8E–09	5.7E–09	7.7E–09	9.6E–09	1.1E–08	1.3E–08	1.5E–08	1.7E–08	1.9E–08	2.9E–08	3.8E–08	4.8E–08	5.7E–08	6.7E–08	7.7E–08	8.6E–08	9.6E–08
800	1.8E–09	3.6E–09	5.4E–09	7.2E–09	8.9E–09	1.1E–08	1.3E–08	1.4E–08	1.6E–08	1.8E–08	2.7E–08	3.6E–08	4.5E–08	5.4E–08	6.3E–08	7.2E–08	8.1E–08	8.9E–08
900	1.7E–09	3.4E–09	5.1E–09	6.7E–09	8.4E–09	1.0E–08	1.2E–08	1.3E–08	1.5E–08	1.7E–08	2.5E–08	3.4E–08	4.2E–08	5.1E–08	5.9E–08	6.7E–08	7.6E–08	8.4E–08
1000	1.6E–09	3.2E–09	4.8E–09	6.4E–09	8.0E–09	9.6E–09	1.1E–08	1.3E–08	1.4E–08	1.6E–08	2.4E–08	3.2E–08	4.0E–08	4.8E–08	5.6E–08	6.4E–08	7.2E–08	8.0E–08

established fairly easily [12,14,122,177]. The conventional idea is that the sum of twice the thickness of the sheath plus the thickness of the negative glow as a function of the pressure defines the minimum and maximum conditions for HCD. However, the thickness of the sheath depends on the gas pressure in a very complicated way and the thickness of the negative glow depends on the density of atoms (the gas pressure) and the interaction (ionization and excitation) cross section and this strongly depends on the electron energy [178].

Studies of atmospheric microplasmas and other high-pressure hollow cathode devices have reported that the maximum value of *p.d* for HCD is approximately 5–6 Torr cm, implying that the high-pressure limit is inversely proportional to the actual operating gas pressure. The upper *p.d* limit is also dependent on the type of gas used [134]. Furthermore, for a given value of *p.d* and discharge current, the operating voltage has been shown to be lower for smaller values of *d* [18,140,179]. However, this cannot be explained in terms of a constant current density, since when the area of the cathode was decreased by a factor of four the operating voltage decreased by between 20 and 30%, depending on the length of the hollow cathode. Additionally, a study [180] showed that the discharge voltage decreased with increasing gas flow [181]. In contrast, A.S. Metel (1984) showed that the minimum pressure for the HCD state is proportional to the ratio of the area of the output aperture of the cathode to the internal cathode surface area [182]. The minimum operating pressure was seen to decrease to 10^{-2} Pa (0.075 mTorr) as the ratio decreased to 10^{-3}. This ratio was considered to describe the ease with which high-energy electrons could escape from the cathode. A review of hollow cathode spectral lamps [183] reported that the minimum pressure *p* for the HCD state increased as the cathode diameter *d* decreased, such that: *d* [mm] = *cp* [mTorr], in which *c* varied from 0.5 to 10 depending on the cathode material.

Earlier models and explanations [12–14,30,123,124] of the hollow cathode effect proposed that the upper limit of the *p.d* product corresponded to the point at which the electron energy loss was such that the electrons were no longer reflected back to the negative glow region from the opposing cathode sheath (no pendulum oscillation) and therefore, additional ionization events did not occur. The explanation of the lower limit has been less precise, it is known [126,127,184] that the sheath–presheath distance increases as the pressure decreases, and the ionization probability also decreases, but no clear model of why the hollow cathode stops as the pressure or cathode diameter decreases below the threshold value has been proposed. The situation is somewhat clearer for the present model involving the generation of doubly-charged ions. The interval between upper and lower *p.d* limits corresponds to the conditions when there exists a significant population of electrons with sufficient energy to produce secondary ionization of the inert gas atoms (~25 eV for Ar), together with a sufficient density of singly-charged Ar^+ ions in the negative glow region. If the pressure is too high, or the diameter too large, then the concentration, or flux, of "high" energy electrons into the negative glow is too small to generate the HCD state. If the pressure is too low, then the concentration of Ar^+ ions in the negative glow is insufficient to allow the formation of a significant population of Ar^{2+} ions, and therefore HCD cannot exist. If the diameter is too small, then the thin negative glow region can have an appreciable electric field that accelerates the singly-ionized ions toward the cathode fall (presheath) and reduces their concentration such that the secondary ionization process is no longer possible. If the diameter is large, a higher voltage is required to produce a sufficient number of high-energy electrons in the centre of the negative glow region to generate the Ar^{2+} ions.

Table 4
The darker shaded area (13.56 MHz RF) and the lighter shaded area (a 200 ns negative DC pulse) correspond to times for which the electron energy (electron velocity) is sufficiently large for passage of an electron from the cathode surface to the centre of the cathode; as required for the doubly ionized theory.

Electron energy (eV)	Time [s] for an electron to travel from the cathode surface to the cathode centre																	
	Cathode diameter (m)																	
	0.01	0.02	0.03	0.04	0.05	0.06	0.07	0.08	0.09	0.1	0.15	0.2	0.25	0.3	0.35	0.4	0.45	0.5
1	8.4E−09	1.7E−08	2.5E−08	3.4E−08	4.2E−08	5.1E−08	5.9E−08	6.7E−08	7.6E−08	8.4E−08	1.3E−07	1.7E−07	2.1E−07	2.5E−07	3.0E−07	3.4E−07	3.8E−07	4.2E−07
2	6.0E−09	1.2E−08	1.8E−08	2.4E−08	3.0E−08	3.6E−08	4.2E−08	4.8E−08	5.4E−08	6.0E−08	8.9E−08	1.2E−07	1.5E−07	1.8E−07	2.1E−07	2.4E−07	2.7E−07	3.0E−07
3	4.9E−09	9.7E−09	1.5E−08	1.9E−08	2.4E−08	2.9E−08	3.4E−08	3.9E−08	4.4E−08	4.9E−08	7.3E−08	9.7E−08	1.2E−07	1.5E−07	1.7E−07	1.9E−07	2.2E−07	2.4E−07
4	4.2E−09	8.4E−09	1.3E−08	1.7E−08	2.1E−08	2.5E−08	3.0E−08	3.4E−08	3.8E−08	4.2E−08	6.3E−08	8.4E−08	1.1E−07	1.3E−07	1.5E−07	1.7E−07	1.9E−07	2.1E−07
5	3.8E−09	7.5E−09	1.1E−08	1.5E−08	1.9E−08	2.3E−08	2.6E−08	3.0E−08	3.4E−08	3.8E−08	5.7E−08	7.5E−08	9.4E−08	1.1E−07	1.3E−07	1.5E−07	1.7E−07	1.9E−07
6	3.4E−09	6.9E−09	1.0E−08	1.4E−08	1.7E−08	2.1E−08	2.4E−08	2.8E−08	3.1E−08	3.4E−08	5.2E−08	6.9E−08	8.6E−08	1.0E−07	1.2E−07	1.4E−07	1.5E−07	1.7E−07
7	3.2E−09	6.4E−09	9.6E−09	1.3E−08	1.6E−08	1.9E−08	2.2E−08	2.6E−08	2.9E−08	3.2E−08	4.8E−08	6.4E−08	8.0E−08	9.6E−08	1.1E−07	1.3E−07	1.4E−07	1.6E−07
8	3.0E−09	6.0E−09	8.9E−09	1.2E−08	1.5E−08	1.8E−08	2.1E−08	2.4E−08	2.7E−08	3.0E−08	4.5E−08	6.0E−08	7.5E−08	8.9E−08	1.0E−07	1.2E−07	1.3E−07	1.5E−07
9	2.8E−09	5.6E−09	8.4E−09	1.1E−08	1.4E−08	1.7E−08	2.0E−08	2.2E−08	2.5E−08	2.8E−08	4.2E−08	5.6E−08	7.0E−08	8.4E−08	9.8E−08	1.1E−07	1.3E−07	1.4E−07
10	2.7E−09	5.3E−09	8.0E−09	1.1E−08	1.3E−08	1.6E−08	1.9E−08	2.1E−08	2.4E−08	2.7E−08	4.0E−08	5.3E−08	6.7E−08	8.0E−08	9.3E−08	1.1E−07	1.2E−07	1.3E−07
20	1.9E−09	3.8E−09	5.7E−09	7.5E−09	9.4E−09	1.1E−08	1.3E−08	1.5E−08	1.7E−08	1.9E−08	2.8E−08	3.8E−08	4.7E−08	5.7E−08	6.6E−08	7.5E−08	8.5E−08	9.4E−08
30	1.5E−09	3.1E−09	4.6E−09	6.2E−09	7.7E−09	9.2E−09	1.1E−08	1.2E−08	1.4E−08	1.5E−08	2.3E−08	3.1E−08	3.9E−08	4.6E−08	5.4E−08	6.2E−08	6.9E−08	7.7E−08
40	1.3E−09	2.7E−09	4.0E−09	5.3E−09	6.7E−09	8.0E−09	9.3E−09	1.1E−08	1.2E−08	1.3E−08	2.0E−08	2.7E−08	3.3E−08	4.0E−08	4.7E−08	5.3E−08	6.0E−08	6.7E−08
50	1.2E−09	2.4E−09	3.6E−09	4.8E−09	6.0E−09	7.2E−09	8.4E−09	9.5E−09	1.1E−08	1.2E−08	1.8E−08	2.4E−08	3.0E−08	3.6E−08	4.2E−08	4.8E−08	5.4E−08	6.0E−08
60	1.1E−09	2.2E−09	3.3E−09	4.4E−09	5.4E−09	6.5E−09	7.6E−09	8.7E−09	9.8E−09	1.1E−08	1.6E−08	2.2E−08	2.7E−08	3.3E−08	3.8E−08	4.4E−08	4.9E−08	5.4E−08
70	1.0E−09	2.0E−09	3.0E−09	4.0E−09	5.0E−09	6.1E−09	7.1E−09	8.1E−09	9.1E−09	1.0E−08	1.5E−08	2.0E−08	2.5E−08	3.0E−08	3.5E−08	4.0E−08	4.5E−08	5.0E−08
80	9.4E−10	1.9E−09	2.8E−09	3.8E−09	4.7E−09	5.7E−09	6.6E−09	7.5E−09	8.5E−09	9.4E−09	1.4E−08	1.9E−08	2.4E−08	2.8E−08	3.3E−08	3.8E−08	4.2E−08	4.7E−08
90	8.9E−10	1.8E−09	2.7E−09	3.6E−09	4.4E−09	5.3E−09	6.2E−09	7.1E−09	8.0E−09	8.9E−09	1.3E−08	1.8E−08	2.2E−08	2.7E−08	3.1E−08	3.6E−08	4.0E−08	4.4E−08
100	8.4E−10	1.7E−09	2.5E−09	3.4E−09	4.2E−09	5.1E−09	5.9E−09	6.7E−09	7.6E−09	8.4E−09	1.3E−08	1.7E−08	2.1E−08	2.5E−08	3.0E−08	3.4E−08	3.8E−08	4.2E−08
200	6.0E−10	1.2E−09	1.8E−09	2.4E−09	3.0E−09	3.6E−09	4.2E−09	4.8E−09	5.4E−09	6.0E−09	8.9E−09	1.2E−08	1.5E−08	1.8E−08	2.1E−08	2.4E−08	2.7E−08	3.0E−08
300	4.9E−10	9.7E−10	1.5E−09	1.9E−09	2.4E−09	2.9E−09	3.4E−09	3.9E−09	4.4E−09	4.9E−09	7.3E−09	9.7E−09	1.2E−08	1.5E−08	1.7E−08	1.9E−08	2.2E−08	2.4E−08
400	4.2E−10	8.4E−10	1.3E−09	1.7E−09	2.1E−09	2.5E−09	3.0E−09	3.4E−09	3.8E−09	4.2E−09	6.3E−09	8.4E−09	1.1E−08	1.3E−08	1.5E−08	1.7E−08	1.9E−08	2.1E−08
500	3.8E−10	7.5E−10	1.1E−09	1.5E−09	1.9E−09	2.3E−09	2.6E−09	3.0E−09	3.4E−09	3.8E−09	5.7E−09	7.5E−09	9.4E−09	1.1E−08	1.3E−08	1.5E−08	1.7E−08	1.9E−08
600	3.4E−10	6.9E−10	1.0E−09	1.4E−09	1.7E−09	2.1E−09	2.4E−09	2.8E−09	3.1E−09	3.4E−09	5.2E−09	6.9E−09	8.6E−09	1.0E−08	1.2E−08	1.4E−08	1.5E−08	1.7E−08
700	3.2E−10	6.4E−10	9.6E−10	1.3E−09	1.6E−09	1.9E−09	2.2E−09	2.6E−09	2.9E−09	3.2E−09	4.8E−09	6.4E−09	8.0E−09	9.6E−09	1.1E−08	1.3E−08	1.4E−08	1.6E−08
800	3.0E−10	6.0E−10	8.9E−10	1.2E−09	1.5E−09	1.8E−09	2.1E−09	2.4E−09	2.7E−09	3.0E−09	4.5E−09	6.0E−09	7.5E−09	8.9E−09	1.0E−08	1.2E−08	1.3E−08	1.5E−08
900	2.8E−10	5.6E−10	8.4E−10	1.1E−09	1.4E−09	1.7E−09	2.0E−09	2.2E−09	2.5E−09	2.8E−09	4.2E−09	5.6E−09	7.0E−09	8.4E−09	9.8E−09	1.1E−08	1.3E−08	1.4E−08
1000	2.7E−10	5.3E−10	8.0E−10	1.1E−09	1.3E−09	1.6E−09	1.9E−09	2.1E−09	2.4E−09	2.7E−09	4.0E−09	5.3E−09	6.7E−09	8.0E−09	9.3E−09	1.1E−08	1.2E−08	1.3E−08

Several groups have shown that the length of the cathode also plays an important role in discharge characteristics [48,140,152,185–189]. One study [190] showed that for a 4-mm-diameter cathode operated at 2.3 kPa (17 Torr, $p.d$ ~6.9 Torr cm) the optimum length of the cathode for a uniform axially-excited atom density (plasma density) was 20 mm. For longer cathodes, a strong axial non-uniformity in the plasma density was found with two maxima near the exit of each end of the cathode and a minimum in the central region. The I–V characteristics of the discharge showed little change as the length was increased from 20 to 50 mm implying that only the two regions of maximum plasma density were active and the increased central area between the two maxima did not contribute to the plasma current. The discharge in a 10-mm-long cathode was stable but significantly higher voltages were needed to generate the same current that was obtained with the 20 mm version, again showing that the active area of the cathode was very important for the production of electrons and ions.

Reference [152] reported that the ratio of the length to the radius of the cathode should not exceed 14, while reference [36] suggested 7–10 for this ratio. The study [185] reported that the relative loss of fast electrons through the aperture of the cathode increased as the cathode length was reduced and that this increased loss raised the minimum pressure limit at which the HCD state could be established. The addition of an electron reflector or an appropriate magnetic field was found to again lower the minimum operating pressure of the hollow cathode. The HCD state could be easily sustained for ratios of the aperture area to the internal area of the cathode of less than 0.2. For smaller values of the ratio, the I–V characteristics of the discharge were almost independent of the ratio. However, for ratio values greater than 0.2, the applied voltage had to be increased considerably to maintain the current; the plasma changed into the D-HC state. Other studies have indicated that the loss of ions, from the low-field negative glow region, through the ends of the hollow cathode can also be important in quenching the HCD state [128].

6. Dependence on electrical supply: DC, RF or P-DC

As discussed earlier, the conventional theory of the hollow cathode effect involves multiple sheath-to-sheath electron oscillations. Obviously, for the HCD condition to exist, such a process must take place in a time less than half the period of the RF cycle, 37 ns, when the electrode is negative. This means that for a hollow cathode of a given diameter, there is a minimum electron velocity (energy) for the hollow cathode effect to occur. Similarly, if pulsed DC, P-DC, is used, then only energies and diameters that result in times shorter than the duration of the negative pulse are allowable. Table 3 shows the time required for an electron to perform three sheath-to-sheath oscillations as a function of the electron energy and the cathode diameter; the darker shaded background highlights the allowable times for RF excitation of electrons and the lighter shaded regions correspond to times shorter than 200 ns; a commonly used value of the pulse length in P-DC experiments. This is, of course, a simplification of the real situation since the electron velocity would oscillate between zero at each extreme to an almost constant maximum value within the central negative glow region. Table 4 shows similar data, but in agreement with the present model that the hollow cathode effect involves electrons travelling from the surface of the cathode to the centre of the cylinder.

If we assume that the electron energy is proportional to the applied voltage and if we therefore concentrate our attention on the energy range 200–400 eV, it can be seen that for the conventional pendulum model there is quite a notable limitation on the cathode diameters

that can be used, independent of the gas pressure. For RF, the quasi-resonant hollow-cathode discharge should not exist for cathode diameters of 20 cm, or larger. However, using the present model based on the formation of doubly ionized ions, the HCD effect should be possible for 50 cm diameter cathodes, or larger. Unfortunately, there are very few experimental studies of the formation of the true HCD state using RF. Many reports involving the use of RF and cold cathodes do not present clear evidence that the discharge is in the HCD, rather than D-HC mode. Furthermore, most RF hollow cathode articles use cathode diameters less than 10 cm [139,191–193]. The cathode diameter limitation for P-DC is much less and if pulse lengths longer than 200 ns are used, the discharge appears to be very similar to a DC discharge [122,194].

Pulsed DC has been extensively studied for hollow cathode gas-flow sputtering systems and it has been reported that the rate of current increase versus voltage was similar for both DC and P-DC. However, under the same conditions, the voltage required to create the high-density plasma was significantly lower for the P-DC excitation [22,180].

7. Magnetic field effect

In general terms, the application of a magnetic field along the axis of the hollow cathode has an effect similar to that of a magnetron cathode. The idea is that if the magnetic field is applied perpendicular to the electric field, then the electrons adopt a helical trajectory and this extended path length increases the probability of ionization events. In the case of the planar magnetron, it is clear how the trapping of the electrons in a helical trajectory can be beneficial. The field intensity needs to be such that the electrons are trapped near the presheath, i.e. close to the edge of the negative glow, so that the additional ions produced are accelerated by the full sheath potential. Since in the hollow cathode, electrons are not as easily lost to ground as in the case of the planar magnetron, it is not completely clear how the magnetic field increases ionization. However, the use of magnetic fields has been reported to increase the plasma density and, correspondingly, the plasma current [195–204].

Additionally, it has been found that above a certain threshold value, the effect of the magnetic field saturates and it was proposed that the magnetic field could be beneficial only while the Larmor radius of the electrons was less than the sheath thickness. Under these conditions, the electrons are confined close to the cathode surface and fundamentally alter the structure and parameters of the sheath [3,195,196,199,205,206].

8. Use of hollow cathodes in the synthesis of thin films

Hollow cathodes are used in a wide variety of applications: as efficient light sources [23], as sources of electrons [207–213] to generate excited species for elemental analysis [1,152,183,214], as ion sources [3,199,215–219], for nitriding [220–223], space propulsion [224–226], vacuum welding [227], basic plasma research [228,229], cluster formation [230] and plasma-activated pre-treatment and coating processes [231–233] among others.

8.1. Review publications

Several review articles have been published on hollow cathodes.

The hollow-cathode effect and the theory of glow discharges, 1954 [13]. This is a study of the electric field between parallel plate cathodes with a good summary of earlier work. The article concludes that UV emission from the plasma was an “essential factor in secondary electron emission”. The article includes 53 references.

Hollow cathode arcs, 1974 [26]. The paper clearly describes the operation and working regimes of hollow-cathode arcs, the variation of the discharge properties along the cathode, the interdependence between the cathode sheath voltage and the gas flow, the use of magnetic fields and the rotation and oscillation of the arc. Various applications of the HCA are listed. The paper incorporates 119 references.

Magnetron sputtering: basic physics and application to cylindrical magnetrons, 1978 [234]. This is a concise presentation of the basic principles underlying the operation of DC magnetron sputtering sources, with emphasis on cylindrical magnetrons including hollow cathodes. The paper includes 90 references.

Theory of the hollow cathode arc, 1978 [27]. A fairly complete description of the physical processes involved in HCA, including the radial and axial variation of the plasma parameters and the axial variation of the gas pressure and wall temperature. The study demonstrates the importance of the field-enhanced thermionic effect for electron emission from the cathode and that the cathode wall is mainly heated by ion bombardment. The study includes 27 references.

A critical review of spectral and related physical properties of the hollow cathode discharge, 1981 [24]. This paper summarizes the previous 50 years of work on the electrical characteristics of the DC hollow cathode discharge. The densities and energies of the electrons and positive ions found in hollow cathode cavities are discussed in relation to the spectral line intensities of the carrier gas and atoms sputtered from the cathode. The review includes reports the existence of significant amounts of high-energy doubly-charged argon ions and the radial distribution of the different charge particles. This work contains 68 references.

Hollow Cathode Discharges, 1984 [21]. The article covers both hollow cathode and Grimm type discharges [235] used for glow discharge optical emission spectroscopy. The paper includes a good description of the fundamental properties of the glow discharge and sputtering phenomena, together with a description of the importance of the geometry of the cathode and many applications. The article has 690 references.

Hot hollow cathode and its applications in vacuum coating: A concise review, 1986 [236]. A clear description of the conventional hollow cathode effect is given. Both cold and hot discharges are described and the characteristics of two examples of thin films deposited using hollow cathode discharges are presented. The paper includes 69 references.

Hollow cathode etching and deposition, 1988 [237]. The main theme of this paper is the good selectivity and etching characteristics provided by the HC discharge. However, deposition of polymers, SiO_2 and Si is also described. The study contains 41 references.

The study of the physics of hollow cathode discharges, 1993 [25]. The study concludes that photoelectron emission from the cathode cannot explain the I–V characteristics of the hollow cathode effect. The paper includes 31 references.

Radio frequency hollow cathodes for plasma processing technology, 1996, [139] and *Thin film processing by radio frequency hollow cathodes*, 1997 [192]. These two reports contain very similar information. They summarize the principal features of RF hollow cathode discharges; both HCD and HCA. The studies consider that metastable excited atoms act as an additional heat source enhancing thermionic electron emission and ionization of the gas. In the case of the HCA, it was reported that the discharge could be sustained with the sputtered metal ions and no additional gas. Examples are included of PECVD and PVD processes, and magnetic focussing in a linear hollow cathode system. 52 and 32 references are included, respectively.

High-pressure hollow cathode discharges, 1997 [120]. This paper includes a good description of the *p.d* relation for hollow cathode operation leading to the explanation of the operation of micro-HCs at high pressures. The article contains 23 references.

Review: Gas discharge plasmas and their applications, 2002 [238]. This work provides a concise overview of DC, pulsed DC, RF, and microwave glow discharges, various types of atmospheric plasmas and low-pressure high-density plasmas in different forms, including electron cyclotron resonators (ECRs), helicon sources, inductively-coupled plasmas (ICPs) and expanding jets. An extensive list of

Table 5
Publications of thin film synthesis by gas-flow sputtering in a hollow cathode. The target material and sputtering gases are given in the left column. In cases for which reactive gas was remotely added to the discharge, this is also listed.

Deposited material [Solid material/source gas]	Deposition rate	Substrate (ND) = not defined	Comments	Refs. (year)
Fe [Fe/Ar]	13,000 nm/min	Glass	DC probably arc, 666 Pa, 370 V/0.5 A, T_{subs} >500 °C.	[268] (1987)
Fe, Ti, Cu [Metal/Ar]	130 nm/min (Fe), 420 nm/min (Cu), 74 nm/min (Ti)	Glass, Si (ND)	Cathode/anode/...../cathode/anode construction. Not cooled → probably arc. 666 Pa, <160 W (DC), T_{subs} ~380 °C from plasma heating. Good film adhesion.	[268,270] (1987, 1988)
Cu, Fe, Ti [Metal/Ar]	420 nm/min (Cu), 160 nm/min (Fe, 74 nm/min) (Ti) depending on the gas flow & plasma power	Glass	DC HC water-cooled, 133 Pa, 1.5 A, 350 V (Cu), 320 V (Fe), 250 V (Ti), T_{subs} 250 °C (Cu & Ti), 190 °C (Fe).	[270,271] (1989)
YBaCuO [YBaCu/Ar with O_2]	1.1–2.3 nm/min	Cu coated Si, MgO (100)	Linear water-cooled HC, DC 260 V/0.3 A, pressure 300–400 Pa, T_{subs} 710–800 °C. Good superconductors.	[156,272] (1991, 1996)
Cu, $YBa_2Cu_3O_{7-x}$ [Cu or YBaCu/Ar]	50 nm/min (Cu), 2.3 nm/min (YBCO)	YSZ (001), $SrTiO_3$ (100)	DC HC water cooled. For Cu 0.6 A/380 V. For YBCO 0.6 A/160 V, T_{subs} 500 °C	[156,272] (1991, 1996)
$A1_2O_3$ [Al/Ar + remote O_2]	150 nm/min	Glass	Linear 10 cm HC, 1.4 kW DC, probably arc, 40 Pa.	[139,267] (1996)
Al_2O_3, ZrO_2, TiO_2 [Metal/Ar + remote O_2]	~330 nm/min	Not given	Linear HC 10–47 cm, probably arc, 3–10 kW DC, 40–80 Pa.	[267] (1996)
Ni80Fe20 NPs [NiFe/Ar] Ag film [Ag/Ar]	NPs 4–6 nm	Glass	Two HC sources, NiFe & Ag. Pressure 200 Pa, DC 470 & 110 W, respectively. Gas phase formation of NPs then covered with Ag film.	[273] (1996)
Al, Ti, Zr, Al_2O_3, ZrO_2, TiO_2, TiN YBaCuO [Metal or YBaCu/Ar]	For metals several nm/min (Mo) to μm/min (Pt). 570 nm/min (Ti) 100 nm/min (TiN)	Glass, Si (ND)	Linear & cylindrical HC RF, 280 W, pressure 100 Pa. Adherence of more than 20 N/mm^2.	[139,274] (1996)
Al, Ti, Cr & oxides, nitrides, carbides [Metal/Ar + O_2, N_2, C_2H_2 or CH_4 remote]	60 nm/min (Al), 47 nm/min (Ti), 250–500 nm/min (oxides)	Polyamide, poly-etherether-ketone, epoxy resin, phenol formaldehyde	DC HC arc, −880 V, 2–4 kW, 10–104 Pa. Good wear resistance and film adhesion.	[275] (1998)
Co [Co/Ar]	6 nm/min	Glass	Cylindrical water-cooled HC, DC 470 W, pressure 133 Pa, T_{subs} 75–650 °C. Good quality polycrystalline films.	[276] (1998)
a-C:H(Ti) [Ti/Ar + remote C_2H_2 or CH_4] Ti-C:H (methane)	200 nm/min (C_2H_2) 50 nm/min (CH_4)	Polymers with a metal interlayer	Linear water-cooled HC, DC 700 W, T_{subs} 200 °C, 80 Pa. Films with good wear resistance and hardness. Is a combination of PVD + PECVD.	[277] (1998)
Al, Ti [Al or Ti/Ar or N_2], AlN, Al_2O_3 [Al/Ar + N_2 or O_2]	5 nm/min (Ti) 40 nm/min (Al) 150 nm/min (AlN) 15 nm/min (Al_2O_3)	Si (ND), soda–lime glass	RF cylindrical HC, HCD (medium power) & HC arc (high power). D-HC → HCD transition at a higher power for N_2 & Ti, than for Ar & Al.	[278] (1999)
$CNSi_x$ [Graphite + Si/Ar + CH_4]	High roughness ~2 nm/min, C/N = 0.75 (C_3N_4) for Si <6 at.%	Mo foil	Water-cooled cylindrical HC, RF 400–600 kW, 666 Pa, T_{subs} 600–1100 °C.	[172] (2000)
TiO_xN_y [Ti/Ar + N_2 + O_2]	54 nm/min	Corning glass	HC arc, DC V/A, pressure 6.7 Pa.	[8] (2000)
Al_2O_3, TiO_2, ITO [Metal/Ar + O_2]	400–1000 nm/min (Al_2O_3), 150–1500 nm/min (TiO_2), 500 nm/min (ITO)	Glass, Si(ND)	Linear HC, 40 kW, pressure 50 Pa. Probably HC arc.	[279] (2000)
$YBa_2Cu_3O_{7-x}$, [YBCO/Ar + O_2]	1.1 nm/min with thickness uniformity over 2 in. substrate of 5%	MgO (100)	A 9 cm diam. cylindrical water-cooled HC with a magnetic field. T_{subs} 760 °C at 27 Pa.	[267,280] (2001)
a-Si:H [Si(nozzle)/Ar + H_2]	8–35 nm/min DC films better quality than RF films	Si (ND), quartz	DC & RF HC both cooled & uncooled with magnetic field (200G), −500 to −557 V, 0.5–0.7 A, T_{nozzle} 1000 °C, 267 Pa, T_{subs} 230 °C.	[281,282] (2001, 2002)
AlO_x [Al/Ar × O_2]	10–15 nm/min	Glass placed inside the 2.5 cm diam. HC	Water-cooled HC DC, 600–900 V/0.1–0.15 A, 8.67 Pa.	[283] (2002)
ZnO:Al, ZnO:B, IN_2O_3:(Mo,Zr,W,Nb,Ta,Ti) [Metal/Ar + O_2 remote]	400 nm/min	Soda–lime glass, Si(ND)	Linear water-cooled HC pulsed DC (100 kHz), 180–900 W, pressure 20 Pa, T_{subs} 120–300 °C.	[284,181,285] (2003, 2004, 2005)
TiN [Ti + Ar/N_2] TiO_x [Ti + Ar/O_2] ZnO:Al [Zn:Al + Ar/O_2]	2000 nm/min – 100 nm/min	Si(111), glass	RF linear HC with rotating magnets both arc & HCD, 1.1 kW, 0.67 Pa.	[177,286] (2003, 2009)
Cu, Al, Zn [Metal/Ar]	180–1200 nm/min	Soda–lime glass, Si(ND)	Linear water-cooled HC DC, 300–450 V/0.66–1.5 A, 40 Pa.	[181] (2004)
TiN [Ti/Ar + N_2]	150 nm/min	Si(ND), high-speed steel	RF + microwave hybrid HC arc with magnets, 3 kW (RF) + 1 kW (μW), 0.8 Pa.	[287] (2004)
Ti, Al, Cu & W [Metal/Ar + O_2 remote]	Nanocomposite films with 18.7 nm Ø particles. Rate not given.	Si(100), 100Cr6 steel coated with Al or Ti to improve adhesion.	DC HC probably arc, 650–700 V, 2–4 kW, 20–90 Pa, T_{subs} 200 °C. Good tribological properties.	[288,289] (2004)
a-Si:H, a-Ge:H, a-SiGe:H [2 nozzles Si, Ge + Ar/H_2] GeC [2 nozzles Ge + Ar/H_2 & graphite + Ar]	33–50 nm/min 100 nm/min 25–35 nm/min Not given	Si(100), glass	DC HC water-cooled with a variable magnetic field, 500 V/0.6 A, 0.5 Pa (Si), 500 V/0.45 A, 0.27 Pa (Ge), 650 V/0.75 A, 0.5–2.0 Pa (SiGe), T_{subs} 230–350 °C.	[290–292,241] (2004– 2007)

(continued on next page)

Table 5 (*continued*)

Deposited material [Solid material/source gas]	Deposition rate	Substrate (ND) = not defined	Comments	Refs. (year)
$Pb(Zr_xTI_{1-x})_2O_3$ [Rings of Pb, Zr, Ti/Ar + O_2 remote]	200–250 nm/min	Si(ND) + barrier layers (Si_3N_4 + SiO_2)	Cylindrical HC DC 400–600 V, 40–70 Pa, T_{subs} 230–550–650 °C. Piezoelectric films.	[293–295] (2006, 2007)
NiFe & SmCo [Metals/Ar]	460–1420 nm/min	Glass	DC HC probably arc, 650–700 V, 1.2–2.5 kW, 20–90 Pa, T_{subs} 300–600 °C plasma heating. Hard & soft magnetic film.	[296,297] (2006, 2007)
Fe [Fe/Ar]	15–170 nm diam. by varying conditions. Nanoparticles grow larger with larger HC-to-subs distance.	Glass	DC HC possible arc, T_{gas} ~100 °C, 300 V, 0.2–1.2 A, 130–1300 Pa, HC-to-subs 1.7–7.0 cm.	[298,299] (2006, 2009)
Hydrogen free DLC [Graphite/Ar]	10 nm/min.	Not given	DC HC arc, 110 A, 30–40 V, 0.13 Pa, low gas flow (30 sccm), T_{subs} 400 °C with pulsed DC bias 250–400 V.	[300] (2006)
TiO_2 [Ti + Ar/O_2]	60 nm/min	Si(100)	DC HC no cooling, 310 V/0.3 A, 0.3–0.8 Pa, T_{subs} 100 °C	[301] (2006)
Co_xPt_y [Co tube + Pt chips/Ar]	Not given NPs 5–150 nm diam.	MgO(ND), GaAs	HC DC no cooling probably arc, 1–1.5 A, T_{subs} 300–400 °C, 130–650 Pa.	[302] (2009)
Fe nanoparticles [Fe/Ar] Fe_3O_4 films & nanopillars [Fe + Ar/He + O_2 remote]				
Permalloy 80%Ni/20%Fe [Fe + Ni/Ar]	150–360 nm/min	Glass & Si(100)	Water-cooled cylindrical HC, pulsed DC (250 kHz, 656 ns) 100–250 W, 2.7–8 Pa, T_{subs} <60 °C plasma heating.	[173] (2009)
Ti [Ti/Ar]	22–330 nm/min depending on incident angle & substrate shape	1.4016 (flat) & 1.4301 (pipe, cylinder, etc.) steels	Linear DC HC, 4.5 kW, T_{subs} 320–380 °C, 47 Pa.	[286] (2009)
ZnO:Al [Al–Zn/Ar + remote O_2]	200–300 nm/min decreased with gas pressure, increase with gas flow.	Glass	Water-cooled linear HC, 1.5 kW DC, pressure 50–80 Pa, T_{subs} 50–200 °C.	[303] (2009)
ZnO:Co [Zn + Co/Ar + remote Ar + O_2]	Not given %Co in film depends on how much Co was added inside the HC.	Glass	Cylindrical HC DC 200 W, 130 Pa, T_{subs} 50–100 °C due to plasma heating.	[304,305] (2010)
Cr, CrN [Cr/Ar or AR + N_2]	(P-DC), 2000 nm/min Cr & CrN (RF) 600 nm/min Cr & 2400 nm/min CrN. P-DC Cr less hard than RF Cr films	Si(ND)	Hot cylindrical HC arc, P-DC (250 W) compared to RF, 67 Pa, T_{subs} 350 °C (P-DC) − 300 °C (RF) due to plasma heating.	[193] (2011)
Fe nanoparticles [Fe/Ar]	The NP size and shape (truncated dodecahedron/spherical/cubical) depended on a combination of the deposition time, S–T & gas flow.	Glass or TEM grid.	Cylindrical HC, 1 A/300 V, 1300 Pa. T_{gas} at HC 500 °C. Subs–target separation (S–T) 170–700 mm	[306] (2012)
WO_3 [W/Ar + remote O_2]	268 nm/min 100 times larger than magnetron sputtering	Sn-doped In_2O_3	Water-cooled linear HC, 1 kW DC, pressure 70–90 Pa, T_{subs} <50 °C.	[307] (2013)
Fe & Fe_2O_3 [Fe/Ar + O_2 remote]	10–16 nm/min	Fused silica	Water-cooled cylindrical HC, pulsed DC (100 μs, 600 mA) with RF (15 W). Larger grains & deposition rate than Fe_2O_3 by HIPIMS.	[308] (2013)
Cu nanoparticles [Cu/Ar]	28,200 nm/min 10–40 nm diam.	Not given	Cylindrical HC, pressure 107 Pa, 3 A/30 μs pulses.	[309] (2013)
TiO_2 nanoparticles [Ti/Ar + remote O_2]	NPs <100 nm. Growth depends on temp. gradient target-subs, partial pressure O_2, gas flow & HC current.	Si(111)	Water-cooled cylindrical HC, 0.3 A/320–330 V, 0.3 Pa.	[310] (2013)
Bi nanoparticles [Bi/Ar] Bi/a-C:H nanocomposites [Bi/Ar + CH_4 or C_2H_2 remote]	NPs 10–150 nm diameter, 0.4–4 nm/min Nanocomposites 30–85 nm/min	Glass & Si(100)	Toroidal planar hollow cathode, DC 40–120 W, pressure 6.7–267 Pa, T_{subs} <60 °C plasma heating.	[311] (2013)
C clusters [Graphite/Ar]	Maximum C_2 emission at 2.5 mbar.	Not given	Cylindrical HC, DC 0.5–1.2 kV, pressure 100–350 Pa.	[312] (2014)

applications of gas discharges is given: surface modification, deposition of thin films, etching and substrate cleaning, plasma-immersion ion implantation, surface activation and functionalization, polymerization of polymers, oxidation, nitriding, etc. Finally, light sources including discharge lamps and lasers are described, together with some environmental and biomedical applications. The paper has 196 references.

Plasma and ion sources in large-area coating: A review, 2005 [239]. Using the crucial idea that film properties can be controlled by manipulation of excited and ionized particles incident at the growing film surface, this work explains and describes, with examples, large-area deposition systems based on an extensive number of plasma and ion or electron sources (microwave, RF, DC and pulsed DC) including hollow cathodes. The review includes 130 references.

Review: Ionized physical vapor deposition (IPVD): A review of technology and applications, 2006 [240]. This work concisely describes the development and application of magnetron sputtering systems for ionized physical vapour deposition (IPVD), together with the use of supplementary discharges such as in inductively-coupled plasma magnetron sputtering (ICP-MS), microwave amplified magnetron sputtering, high power impulse magnetron sputtering (HIPIMS), self-sustained sputtering (SSS) and hollow cathode magnetron (HCM) systems. Examples are given to show how IPVD can lead to improved film adhesion, coverage of complex shapes, densification, and control of the plasma chemistry. The article contains 207 references.

Review: Analysis of semiconductor thin films deposited using a hollow cathode plasma torch, 2007 [241]. This review is specific to the use of the hollow cathode discharge to produce hydrogenated amorphous and polycrystalline films of semiconductors by reactive gas flow sputtering. The paper includes 17 references.

Plasma processes at atmospheric and low pressures, 2009 [242] and *Cold atmospheric plasma: Sources, processes, and applications*, 2010 [243]. These similar publications briefly review the primary

Table 6
Publications of thin film synthesis by cathode plasma enhanced chemical vapour deposition using a hollow cathode. The deposited material, solid and gaseous precursors are given in the left column.

Deposited material [Precursors]	Deposition rate	Substrate	Comments	Refs.
Si_3N_4 [$SiH_4 + N_2 + Ar$]	6 nm/min	Si(ND), glass, Fe, Mo, Cu, Al, W, Ge, GaAs	Microwave hollow cathode excitation of N_2, 20–300 Pa, 10–800 W, T_{subs} 50–400 °C	[313] (1985)
Diamond [$CH_4 + H_2$]	17–54 nm/min	Si(100), Mo	Cylindrical HC DC arc, 75–115 V/8 A, 267–3333 Pa, T_{subs} 800–1000 °C	[314] (1988)
a-Si:H [SiH_4] Si_3N_4 [$SiH_4 + Ar + N_2$] in coaxial system	30 μ/min a-Si:H, 1.7 nm/min Si_3N_4	Si(ND), glass + ITO	HC arc cathode inside a quartz tube or coaxial cathode-anode tubes, DC 100 W, 67 Pa, T_{subs} 230 °C.	[315] (1989)
SiO_x:F [$O_2 + SiH_4 + CF_4$]	200 nm/min	Multilayers SiO_x/SiO_x:F/Si	RF, <1 Pa, T_{subs} 250–300 °C.	[316] (1995)
SiO_x:Ge(16–5 mol%) [$SiH_4 + GeH_4 + O_2$]	Not given	Si(ND) with buffer layers	RF 300–600 W, T_{subs} 300–400 °C (plasma heating), 2 Pa.	[317,318] (1996, 1998)
a-Si:H [$Ar + SiH_4 + H_2$], SiN [$Ar + SiH_4 + N_2$], $Si_xO_yN_z$ SiC_x [$Ar + SiH_4 + C_2H_2$], DLC, C [>10%$CH_4 + H_2$], Diamond [<1%$CH_4 + H_2$]	0.5–103 μm/min, 1–103 μm/min, Not given, 1–10 μm/min, <20 μm/min, 10–30 nm/min	Si(ND), glass Si(ND), glass Al, stainless steel Al, stainless steel Si(ND), Mo, W	50–100 Pa, Ts_{ubs} 200 °C 50–100 Pa, T_{subs} 100–500 °C Not given 100 Pa, T_{subs} <300 °C 500–104 Pa, T_{subs} <900 °C 500–104 Pa, T_{subs} <900 °C RF HC arc, >100 W, small cathode used to coat the inside of tubes.	[192] & refs. therein (1997)
Surface modification [O_2]	Not applicable	Polypropylene foil and cellulose membrane	RF linear HC, 600 W, 0.1 Pa (with hollow anode), 1–600 Pa.	[191] (1997)
PTFE-like [$C_4F_8 + Ar$]	15–100 nm/min	Steel, plastic, paper, textiles	Coaxial cathode–anode Ar + remote C_4F_8, RF 50–200 W, 5–100 Pa.	[319,320] (1997, 1998)
a-C:H [CH_4 or C_2H_2 + Ar or He]	Not given	Not given	HC arc + magnetic field 100 G, DC 40 V (Ar)–100 V (He)/20–60 A, 0.3–0.5 Pa. Good plasma studies.	[231] (1999)
CN_x:Si [$CH_4 + N_2$/(Si + graphite)]	<10 nm/min	Mo	RF 400–600 W, 667 Pa, T_{subs} 600–1100 °C. C/N = 3/4 for Si >5 at.%.	[172] (2000)
TiO_x [Titanium tetra-isopropoxide + He + Ar + O_2]	50 nm/min	Si(100), quartz	RF multi-jet HC, 1 kW, T_{subs} 70 °C, 20 Pa.	[321] (2001)
DLC [He thru' HC + CH_4 remote]	70–80 nm/min	Si(111)	RF multi-jet HC, 1 kW, substrate with RF bias (−370 V best hardness), 50–100 Pa.	[322] (2002)
DLC [He + Ar thru' HC + C_2H_2 remote]	100 nm/min	Si(100), stainless steel	RF multi-jet HC water-cooled, 400 W, modulated RF substrate bias (240 W 100 Hz), 20 Pa, T_{subs} 150 °C.	[323] (2002)
DLC, SiC, Si [$CH_4 + C_2H_2 + SiH_4$]	83 nm/min	Steel tubing, Si(ND)	Tubular HC, pulsed DC (2 kHz, 20 μs) 4 kV, coating the inside of tubes. PECVD + external cusp magnetic field, 2 Pa.	[324] (2004)
a-C:H [CH_4]	1–100 nm/min function of $V_{self\text{-}bias}$	Si(100) mounted on one water cooled cathode	RF planar HC, 20–140 W, 1.3–6.7 Pa, $V_{self\text{-}bias}$ −100 to −500 V.	[325] (2007)
DLC [$Ar + C_2H_2$]	20–40 nm/min function of V_{bias}	Ti buffer/stainless steel	RF HC 300 W, 2 Pa, V_{bias} −200 V.	[326] (2008)
$Si:O_x:C_y:H_z$ [Hexamethyl-disoloxane + He + Ar]	1.3–17 nm/min	Si(111), quartz	Remote RF HC coaxial cathode–anode 100–300 W, 3 Pa.	[327] (2008)
SiC/DLC [Si precursor + C_2H_2]	0.1–1 μm/min	304 stainless steel	Bipolar pulsed (<30 μs) DC deposit on the inside of tubes, 0.1–1 kV, 13.3 Pa, T_{sub} 200 °C. Good hardness & corrosion resistance.	[328] (2008)
CN_x [$CH_4 + NH_3$]	Thickness 1 μm, no deposition rate given	Si(ND)	Cylindrical HC, DC 350 V, pressure 1×10^2 Pa, N/C ~0.39.	[329,330] (2008, 2012)
Not defined [Ar + tetramethylsilane]	Rate not given (deposition inside tube)	Stainless steel	Supersonic expansion thru' a HC arc in a tube, >10 Pa, 200 kHz P-DC, D-HC at 50 W/HCD at 150 W. Good study of the importance of the pressure variation.	[331] (2009)
a-CN_x:H [$CH_4 + NH_3 + H_2$]	Not given	Si(ND), quartz	DC HC −350 V, 100 Pa. XPS, UV–Vis & FTIR analysis.	[332] (2009)
DLC [$Ar + C_2H_2$ + tetramethylsilane]	500 nm/min (deposition inside tube)	1020 carbon steel	DC HC 0.1–10 kV, T_{subs} <200 °C, 9.3–16 Pa.	[333] (2009)
SiO_xC_y [Hexamethyl-disiloxane + Ar + N_2O]	Not given	Glass + ITO	RF 50 W PECVD 9.3 Pa. Film hardness increased with increasing N_2O in gas.	[334] (2010)
μC-Si:H [$SiH_4 + H_2$]	40 nm/min @ 200 Pa	Not given	Multi HC RF 5–50 W, 80–330 Pa, T_{subs} 200 °C	[335] (2011)
Si (28 at.%) + C (37 at.%) + O_2 (22 at.%) + H_2 (13 at.%) [Ar + tetramethyl-silane]	1.6 μm/min	Zinc alloy coated steel as cathodes	P-DC, 0.4 Pa, 1.2 kW, corrosion resistant coatings.	[336] (2011)
a-C:H [Ar thru' HC + C_2H_2 + Ar remote]	0.2–1 μm/min (a function of C_2H_2 flow)	Stainless steel, glass, Si(ND) with Ti buffer layer.	DC HC arc with magnetic field (8 Pa), 100 A/20–100 V, DLC @ V_{bias} 200 V + T_{subs} 290 °C, graphite-like @ V_{bias} 200 V + T_{subs} 500 °C, polymer-like @ no V_{bias} + T_{subs} 150 °C.	[160] (2012)
$Si_xO_yF_z$ [$O_2 + SiH_4 + CF_4$]	190 nm/min	Si(100)	RF <200 W, 1.3 Pa, T_{subs} 380 °C. Thick low stress, crack-free graded index films.	[337] (2012)
a-C:H [$Ar + C_2H_2$]	1 μm/min	Stainless steel, glass, Si(ND) with Ti.	Arc PECVD + magnetic field of 8 Pa. 100 A/30–100 V, 0.3 Pa. Ta tube. Polymer-like, diamond-like, graphite-like as a function of substrate bias & T_{subs}.	[160] (2012)

(continued on next page)

Table 6 (*continued*)

Deposited material [Precursors]	Deposition rate	Substrate	Comments	Refs.
a-C + 30–50 at.% Cu + 4–5 at.% H [Ar + C_2H_2]	500 nm/min	Si(100)	Pulsed DC, 450 V/12 A, 60–73 Pa.	[338] (2012)
a-C(N):H [CH_4/H_2 + N_2 or NH_3]	17 nm/min	Si(111), W, Mo	Deposition or erosion in the hollow cathode as a function of N_2 or NH_3 concentration. 8.7–107 Pa.	[339] (2013)
SiO_x [Hexamethyl-disoloxane]	500–3000 nm/min	Polymers, glass	Multiple DC arc PECVD. Pressure 0.5–5 Pa.	[340] (2013)
a-C:H + Cu [C_2H_2 + Ar]	500 nm/min	Not given	Review of high pressure P-DC PECVD, 70–170 Pa.	[341] (2013)
DLC [C_2H_2 + Ar]	17–45 nm/min	Si(100)	Cylindrical or linear HC RF 20–100 W, pressure 0.75–4 Pa, T_{subs} not given.	[342] (2013)
GaN, AlN & $A_{ix}Ga_{1-x}N$ [Ar + trimethylaluminum, trimethylgallium]	Dep rate depends on the ALD cycling.	Si(100) & C-plane sapphire	HC assisted atomic layer deposition, RF 300 W, 20 Pa, T_{subs} 200 °C.	[343,344] (2014)
DLC [C_3H_8 + CH_4 + $Si(CH_3)_2Cl_2$ + H_2]	Not given	Si(100)	Water-cooled cylindrical HC with magnetic field (~80 mT), DC 350–400 V/60–80 mA, 0.8–3.4 Pa. T_{subs} <250 °C plasma heating.	[345] (2014)
DLC [CH_4 + Ar]	29 nm/min	Stainless steel tube	DC HC of stainless steel, 380–420 V/5–8 mA, 20–30 Pa, T_{subs} not given.	[6] (2014)

principles, advantages, and drawbacks of non-equilibrium (cold) atmospheric plasma systems, together with the capabilities and limitations of the atmospheric plasma processing compared with conventional low-pressure plasma processing. An extensive list of cold atmospheric plasma sources is presented, including various systems based on hollow cathodes. 45 and 110 references are included, respectively.

Hollow Cathode Effect in Cold Cathode Fluorescent Lamps: A Review, 2010 [23]. The paper contains a good assessment of the literature on the hollow cathode effect and the conventional models involving the pendulum electrons. The study concluded that the value of the product of gas pressure and cathode diameter used in standard cold cathode fluorescent lamps (CCFL) means that they do not operate using the quasi-resonant hollow cathode effect. The review contains 17 references.

8.2. Applications

High-density hollow-cathode plasmas have been employed in several ways for the preparation of thin films and all three variants of the hollow cathode discharge, D-HC, HCD and HCA, have been used. Unfortunately, quite frequently the authors of the reports and publications do not clearly describe which hollow-cathode version is being used.

The high density of electrons and the resulting gas phase collisions can be used as an effective energy source to produce chemical reactions in the precursor gas mixture; as in basic plasma-enhanced chemical vapour deposition (PECVD) type processes. Such processes have been studied when they occur inside the hollow cathode or remotely with the hollow cathode acting as a high flux source of electrons [244,245].

Both electron and ion source variants of the hollow cathode have been used for etching [237,246,247], nitriding [220–223], surface cleaning [177,248] and modification [249–251]. Additionally, hollow cathode discharge and arc systems have been employed as electron sources to enhance the performance of magnetron sputtering in the same way as earlier filament triode sources were used. The use of hollow cathodes in this way was quite popular from the mid 1980s to the mid 1990s [252–255] and a number of patents were awarded [US#4588490 hollow cathode enhanced magnetron sputter device, US#4824544 large area cathode lift-off sputter deposition device, US#4588490 an etching-deposition system, high plasma density]. However, more recently there have been few new publications. Along similar lines, there have been several papers [156,256,257] about the use of holes in a magnetron sputtering target, or the use of a cylindrical extension surrounding the target, that act as a hollow cathode. In the first case, the idea is that a hollow cathode discharge can be established in the holes and supply electrons and thus enhance the magnetron discharge and therefore the sputtering rate [156,256,258]. In the second version, the magnetron discharge is confined by the extension tube and this increases the plasma density and therefore the sputtering efficiency [257,259–261].

Large-diameter systems have been used to coat electrically-floating substrates placed inside the cylindrical cathodes. An advantage of this arrangement is that sputtering of the interior of the cylindrical target causes the depositing species to arrive at the substrate from all angles and therefore complex shapes can be easily coated very uniformly [234,262–266].

Another sputtering process in a hollow cathode first reported in 1962 [45] has now been developed into the gas-flow sputtering (GFS) technique [267]. Full details were first reported by K. Ishii in 1987 [268], and since then more than 200 articles and approximately 12 patents have been awarded. In fact, there are several forms of the GFS system independent of whether they use DC, RF or P-DC [269];

If the cathode is not cooled, then the discharge is normally a high-density high temperature arc.Some studies have involved systems with axial magnetic fields.

Reactive sputtering has been carried out in which the reactive gas is passed through the hollow cathode or, to reduce reaction with the cathode surface, the reactive gas is added in the remote afterglow area at the outlet of the cathode.

Linear planar cathodes have been developed to coat large areas, with or without stationary or varying magnetic fields.

The common principal is that atoms sputtered from one area of the cathode wall, rather than just depositing on the opposing wall segment, are entrained by the high gas flow toward the exit of the cathode. In this way the gas flow, as well as the plasma power, can be used to control the deposition rate. For the cold cathode versions, the useable pressure range for high efficiency use is limited by the *p.d* restrictions discussed earlier. However, several articles [21,23,234] have reported the use of hollow cathodes under conditions where the quasi-resonant HCD state does not occur, but the increased plasma density found for the D-HC status is nevertheless sufficient to give beneficial results.

Tables 5 and 6 provide an extensive and approximately chronological selection of the reports of thin film synthesis, the conditions used and the range of deposition rates found for GFS and PECVD processes in hollow cathode systems. The left column includes the target or precursor material and sputtering or source gas used.

9. Conclusions

In this review, we described the three types of discharges that are observed in a hollow cathode: 1) the high-voltage, low-current low-density plasma that we refer to as a discharge in a hollow cathode D-HC, 2) the quasi-resonant high-current discharge, which we have called the hollow cathode discharge HCD, and 3) the low-voltage, high-current hollow cathode arc HCA. We used the basic concepts of plasma physics, particularly the gas phase and cathode surface excitation and ionization collision processes, to describe the structure of a typical parallel-plate DC discharge. Here we explained how published data have shown that the luminosity of the cathode glow is primarily due to ion-impact rather than electron-impact excitation. This idea implies that the energy of the majority of the electrons in the cathode sheath is less than about 25 eV between the cathode and the edge of the negative glow, greater than this value inside the negative glow region and is again less than ~25 eV from the border of the negative glow region to throughout most of the Faraday dark space.

The conventional theory of operation of the hollow cathode discharge, based on the existence of "pendulum" electrons, was presented and some inconsistencies of the model were discussed. In addition, the importance of combined thermionic-field electron emission process from hot cathodes was described as an explanation of the characteristics of cathode arcs.

Using data from a description of the structure of a DC discharge together with published values of secondary electron emission coefficients for singly- and doubly-charged noble gas ions, we presented a new model of the quasi-resonant hollow cathode discharge based on the formation of doubly-charged ions within the negative glow region. The basic hypothesis is that inside the negative glow the concentrated flux of relatively high-energy electrons, together with the accumulation of singly-charged ions, gives rise to the formation of doubly-charged ions. Since the secondary electron emission coefficient of these ions is approximately 4 times greater than that of singly-charged ions, the generation of doubly-charged ions strongly enhances the production of electrons from the cathode and this, in turn, produces more ions including additional doubly-charged ions. This quasi-resonant process explains the super-linear increase in the plasma density, plasma current and light emission of the discharge as the hollow cathode discharge condition is established. The effect of: the cathode geometry, the gas pressure/cathode-diameter product, the use of a pulsed-DC or RF power supplies and a magnetic field was discussed in light of the new discharge model.

An important implication of the new model is that a hydrogen quasi-resonant hollow cathode discharge should not be possible. To study this, we performed hollow cathode discharge experiments in argon, helium and hydrogen, using the same conditions of plasma power, gas pressure and flow. A quasi-resonant discharge was observed for argon and helium but only a low-density, low-current plasma could be formed in hydrogen.

A collection and brief description of most of the previous hollow cathode review papers has been included and an extensive chronological catalogue of reports describing the deposition of thin films using gas-flow sputtering and plasma-enhanced chemical vapour deposition in hollow cathode systems is presented.

Finally, the foremost characteristics of hollow cathode discharges that make them of particular interest for coating applications are;

1) Plasma densities in excess of 10^{10} cm^{-3}:
   - This can provide high optical emission intensities.
   - An intense flux of either electrons or ions can be extracted.
   - Plasma chemical reactions for deposition, surface modification, or etching can be strongly enhanced.
   - Compared to magnetron sputtering, a larger fraction of sputtered atoms is ionized; for magnetron sputtering $M^+/M \leq 0.01$ [78,346] and for sputtering with a hollow cathode $M^+/M \leq 0.2$ [250,259,260,269].
2) Since relatively high gas pressures are often used, the average electron temperature is typically a few eV [347], but compared to planar sputtering discharges the ion energies can be significantly higher [51], leading to relatively high gas temperatures.
   - Plasma/gas heating of the substrate is important and, therefore, the film properties often depend on the cathode-to-substrate distance, as well as the plasma power used.
   - The above, together with the high plasma density, further enhances the rate of reactive chemical reactions.
3) Both the electrons and ions are accelerated by the intense sheath, but velocities of both species are, in general, perpendicular to the cathode surface and not toward the exit of the hollow cathode.
   - This, together with the high gas pressure, means that, without applying a negative substrate bias, there is little intrinsic bombardment of the substrate [294].
4) The sputtered atoms travel from wall to wall within the hollow cathode.
   - A high gas flow can be used to entrain the atoms out of the cathode to the substrate, as in gas-flow sputtering, and therefore provides a way to control the deposition rate that is independent of the plasma parameters.
5) Under the quasi-resonant condition of HCD, an appreciable concentration of doubly-charged ions will be present in the discharge.
   - For the same electric field, doubly-charged ions have twice the energy of a singly-charged ion, can sputter the target at a much higher rate and give rise to much larger (super-linear) secondary electron emission yields [348,349].

Acknowledgements

The authors wish to acknowledge the financial backing of the UNAM-DGAPA project #IN112111 and the considerable support provided by our friends and colleagues, particularly, Dr. Joe Greene of the University of Illinois, USA, Linköping University, Sweden, and the National Taiwan Univ. of Science and Technology, and in Mexico; Dr. Enrique Camps of ININ, Dr. Sandra Rodil of IIM-UNAM and Dr. Citlali Sanchez-Ake, Dr. Crescencio Garcia-Segundo and Dr. Mayo Villagran of CICADT-UNAM, as well as many of the students associated with the PlasNaMat group of the IIM-UNAM and Dr. Lloyd Richardson for his help revising and correcting the text of the article.

References

[1] A. Qayyum, M.I. Mahmood, Anal. Chim. Acta 606/1 (2008) 108.
[2] V.L. Galansky, V.A. Gruzdev, I.V. Osipov, N.G. Rempe, J. Phys. D. Appl. Phys. 27 (1994) 953.
[3] E.M. Oks, A. Anders, I.G. Brown, Rev. Sci. Instrum. 75/4 (2004) 1030.
[4] E.U. Biborosch Dieter-Leopold, P. Gheorghe, F. Klaus, J. Plasma Fusion Res. Ser. 4 (2001) 297.
[5] A.C.J.P.V.H. Baggio-Scheid, J.W. Neri, Braz. J. Phys. 33/2 (2003) 336.
[6] S. Li, F. He, Q. Guo, J. Ouyang, Plasma Sci. Technol. 16/1 (2014) 63.
[7] Z. Donko, K. Rozsa, M. Janossy, J. Phys. D. Appl. Phys. 24 (1991) 1322.
[8] M.H. Kazemeini, A.A. Berezin, N. Fukuhara, Thin Solid Films 372 (2000) 70.
[9] D.M. Goebel, I. Katz, Hollow Cathodes, Fundamentals of Electric Propulsion: Ion and Hall Thrusters, JPL Space Science and Technology SeriesChap 6 2008.
[10] T.P. Mollart, Ph.D. Thesis, Durham University, UK, 1993.
[11] F. Paschen, Ann. Phys. 355/16 (1916) 901.
[12] L.M. Lidsky, S.D. Rothleder, D.J. Rose, S. Yoshikawa, C. Michelson, R.J. Mackin, J. Appl. Phys. 33/8 (1962) 2490.
[13] P.F. Little, A.v. Engel, Proc. R. Soc. Lond. A Math. 224/1157 (1954) 209.
[14] A.D. White, J. Appl. Phys. 30/5 (1959) 711.
[15] G. Franz, Low Pressure Plasmas and Microstructuring Technology, Springer, 2009.
[16] W. Kohsiek, Plasma Phys. 17 (1975) 1083.
[17] L. Warren, Ph.D. Thesis, Lawrence Radiation Laboratory, University of California, CA, USA, 1968.
[18] D.B. Mihailova, Ph.D. Thesis, Technische Universiteit Eindhoven, The Netherlands, 2010.
[19] V.M. Rashkovan, I.A. Ponomaryova, J. Phys. D. Appl. Phys. 38/16 (2005) 2817.

[20] K.H. Schoenbach, L.L. Vahala, G.A. Gerdin, N. Homayoun, F. Loke, G. Schaefer, in: M. Gundersen, G. Schaefer (Eds.), Physics and Applications of Pseudosparks, vol. 219, Springer, US, 1990, p. 293.
[21] R. Mavrodineanu, J. Res. Natl. Bur. Stand. 89/2 (1984) 143.
[22] P.K.J. Klusoň, S. Leshkov, M. Chichina, I. Picková, Z. Hubička, M. Tichý, WDS'09 Proceedings of Contributed Papers, 2009, p. 233.
[23] I.L. Alberts, D.S. Barratt, A.K. Ray, J. Disp. Technol. 6/2 (2010) 8.
[24] M.E. Pillow, Spectrochim. Acta B 36 (1981) 821.
[25] A.K. Malik, D.G. Feam, 21st International Electric Propulsion Conference, Electric Rocket Propulsion Society, 1993.
[26] A.R.T.J.-L. Delcroix, Adv. Electron. Electron Phys. 35 (1974) 87.
[27] C.M. Ferreira, J.L. Delcroix, J. Appl. Phys. 49/4 (1978) 2380.
[28] R.V. Kennedy, J. Phys. D. Appl. Phys. 34 (2001) 787.
[29] R.L. Boxman, D.M. Sanders, P.J. Martin, J.M. Lafferty, Handbook of Vacuum Arc Science and Technology: Fundamentals and Applications, Noyes Publications, 1995.
[30] A. Guntherschulze, Z. Tech. Phys. 11 (1939) 49.
[31] G. Stockhausen, M. Kock, J. Phys. D. Appl. Phys. 34 (2001) 1683.
[32] F.F. Chen, Introduction to Plasma Physics and Controlled Fusion, Plenum Press, New York, 1984.
[33] G. Francis, Encyclopedia of Physics, 1956.
[34] Y.P. Raizer, Gas Discharge Physics, Springer-Verlag, 1991.
[35] M.A. Lieberman, A.J. Lichtenberg, Principles of Plasma Discharges and Materials Processing, Wiley-Interscience, 2005.
[36] E. Oks, Low-pressure discharges for plasma electron sources, Plasma Cathode Electron Sources, Wiley-VCH Verlag GmbH & Co. KGaA, 2006.
[37] D. Söderström, Ph.D. Thesis, Uppsala University, Sweden (2008).
[38] K.S.S. Harsha, Principles of Physical Vapor Deposition of Thin Films, Elsevier, 2006.
[39] H.S.W. Massey, E.H.S. Burhop, H.B. Gilbody, Electronic and Ionic Impact Phenomena: Recombination and Fast Collisions of Heavy Particles, by H. S. W. Massey and H. B. Gilbody, Clarendon P., 1974
[40] R. Schoen, J.R. Holmes, J. Opt. Soc. Am. 44/6 (1954) 502.
[41] R.B. Brode, Rev. Mod. Phys. 5 (1933) 257.
[42] J.B. Boffard, B. Chiaro, T. Weber, C.C. Lin, At. Data Nucl. Data 93 (2007) 831.
[43] H. Deutsch, K. Becker, A.N. Grum-Grzhimailo, K. Bartschat, H. Summerse, M. Probst, S. Matt-Leubner, T.D. Märk, Int. J. Mass Spectrom. 233 (2004) 39.
[44] A. Surmeian, A. Groza, C. Diplasu, C. Atanasiu, A. Popescu, D. Savastru, M. Ganciu, Rom. Rep. Phys. 65/3 (2013) 869.
[45] T. Musha, J. Phys. Soc. Jpn. 17/9 (1962) 1440.
[46] D. Desideri, M. Bagatin, M. Spolaore, V. Antoni, R. Cavazzana, E. Martines, G. Serianni, M. Zuin, Compel Int. J. Comput. Math. Electr. Electron. Eng. 24/1 (2005) 261.
[47] D.W. Mueller, Nucl. Instrum. Meth. B 42/4 (1989) 467.
[48] U.K.L.D. Tsendin, Electron Kinetics and Applications of Glow Discharges, Springer, 2002.
[49] J.G. Linhart, Plasma Physics, European Atomic Energy Community — EURATOM, Brussels, Belgium, 1969.
[50] N. Baguer, Ph.D. Thesis, Universiteit Antwerpen, Belgium, 2005.
[51] P.M. Martin, Handbook of Deposition Techniques for Films and Coatings, 3rd edition Elsevier, 2010.
[52] H.S. Hwang, J.Y. Oh, Y.S. Kim, S.J. Lee, K.M. Song, H.K. Baik, J. Phys. D. Appl. Phys. 43/49 (2010) 495205.
[53] M.M. Pejovic, G.S. Ristic, IEEE Trans. Plasma Sci. 30/3 (2002) 1315.
[54] A. Fridman, L.A. Kennedy, Plasma Physics and Engineering, Taylor & Francis Books, 2004.
[55] D.M. Mattox, Handbook of Physical Vapor Deposition (PVD) Processing, Film Formation, Adhesion, Surface Preparation and Contamination Control, Noyes, 1998.
[56] D.W. Vance, Phys. Rev. 169/2 (1968) 263.
[57] T. Kawachi, T. Fujimoto, Phys. Rev. E 55/2 (1997) 1836.
[58] D. Rapp, P. Englander-Golden, J. Chem. Phys. 43/5 (1965) 1464.
[59] E. Bultinck, Ph.D. Thesis, Universiteit Antwerpen, Belgium, 2009.
[60] QUANTEMOL, database www.lxcat.net2014.
[61] H.S.W. Massey, E.H.S. Burhop, Electronic and Ionic Impact Phenomena, Oxford University Press, Oxford, 1952.
[62] A. Bogaerts, Ph.D. Thesis, University of Antwerpen, Belgium, 1996.
[63] R.T. Pack, R.B. Walker, B.K. Kendrick, J. Chem. Phys. 109/16 (1998) 6701.
[64] R. Smith, M. Jakas, D. Ashworth, B. Oven, M. Bowyer, I. Chakarov, R. Webb, Atomic and Ion Collisions in Solids and at Surfaces; Theory, Simulation and Applications, Cambridge University, 1997.
[65] H. Zhang, A. Breskin, R. Chechik, S. Shckemelinin, O. Ternyak, E. Cheifetz, Meas. Sci. Technol. 19/5 (2008) 055704.
[66] H.D. Hagstrum, Phys. Rev. 104/2 (1956) 317.
[67] H.D. Hagstrum, Phys. Rev. 104/3 (1956) 672.
[68] F.J. Currell, The Physics of Multiply and Highly Charged Ions, Kluwer Academic Publishers, 2003.
[69] G. Lakits, F. Aumayr, H. Winter, J. Phys. Colloques 50/C1 (1989) C1.
[70] A. Bogaerts, R. Gijbels, Plasma Sources Sci. Technol. 11 (2002) 27.
[71] C. Simon, S. Heuraux, H. Michel, J. Bougdira, M. Fabry, J. Phys. D. Appl. Phys. 24 (1991) 672.
[72] M. Delaunay, M. Fehringer, R. Geller, D. Hitz, P. Varga, H. Winter, Phys. Rev. B 35/9 (1987) 4232.
[73] H. Kurz, F. Aumayr, C. Lemell, K. Töglhofer, H.P. Winter, Phys. Rev. A 48/3 (1993) 2182.
[74] H. Kurz, F. Aumayr, H.P. Winter, D. Schneider, M. Briere, J. McDonald, Phys. Rev. A 49/6 (1994) 4693.
[75] G.L. Cano, J. Appl. Phys. 44/12 (1973) 5293.
[76] R. Decoste, B.H. Ripin, J. Appl. Phys. 50/3 (1979) 1503.
[77] H. Winter, J. Burgdorfer, Slow Heavy-particle Induced Electron Emission from Solid Surfaces, Springer-Verlag, 2007.
[78] G.M. McCracken, Rep. Prog. Phys. 38/2 (1975) 241.
[79] Y. Taga, R&D Review of Toyota CRDL, 28/31993. 1.
[80] D.N. Ruzic, in: S.M. Rossnagel, J.J. Cuomo, W.D. Westwood (Eds.), Handbook of Plasma Processing Technology: Fundamentals, Etching, Deposition and Surface Interactions, Noyes Publications, 1990.
[81] H. Gades, H.M. Urbassek, Appl. Phys. A 61 (1995) 39.
[82] H.F. Beyer, V.P. Shevelko, Introduction to the Physics of Highly Charged Ions, Institute of Physics Publishing, 2003.
[83] B. Feuerbacher, B. Fitton, R.F. Willis, Photoemission and the Electronic Properties of Surfaces, Wiley, Chichester, 1978.
[84] Q.-R. Zhang, Phys. Lett. A 216/1–5 (1996) 125.
[85] J.W.G.H.A. Watson, Principles of Electron Tubes, D. Van Nostrand, 1965.
[86] I.H. Hutchinson, Principles of Plasma Diagnostics, Cambridge University Press, 2002.
[87] H. Conrads, M. Schmidt, Plasma Sources Sci. Technol. 9 (2000) 441.
[88] N.S.J. Braithwaite, Plasma Sources Sci. Technol. 9 (2000) 517.
[89] N. Hershkowitz, Phys. Plasmas 12/5 (2005) 055502.
[90] A. Bogaetts, R. Gijbels, J. Appl. Phys. 78/11 (1995) 6427.
[91] H. Mase, N.Y. Sato, T. Tanabe, T. Ikehata, 25th International Conference on Phenomena in Ionized Gases, 2001.
[92] V. Lisovskiy, V. Yegorenkov, Eur. J. Phys. 30 (2009) 1345.
[93] V.A. Lisovskiy, V.A. Derevianko, V.D. Yegorenkov, Vacuum 103 (2014) 49.
[94] N. Mutsukura, Kenji Kobayashi, Y. Machi, J. Appl. Phys. 68/6 (1990) 2657.
[95] A. Bogaerts, Z. Donko, K. Kutasi, G. Bano, N. Pinhao, M. Pinheiro, Spectrochim. Acta B At. Spectrosc. 55 (2000) 1465.
[96] J.E. Greene, J.M. Whelan, J. Appl. Phys. 44 (1973) 2509.
[97] J.E. Greene, F.S. Osorio, B.G. Streetman, J.R. Nonnan, C.G. Kirkpatrick, Appl. Phys. Lett. 25 (1974) 435.
[98] J.E. Greene, F.S. Osorio, B.R. Natarajan, J. Appl. Phys. 46 (1975) 2701.
[99] J.E. Greene, F.S. Osorio, B.R. Natarajan, J. Vac. Sci. Technol. 12 (1975) 366.
[100] J.E. Greene, F.S. Osorio, J. Vac. Sci. Technol. 10 (1973) 114.
[101] J.E. Greene, J. Vac. Sci. Technol. 15 (1978) 1718.
[102] F.W. Aston, Proc. R. Soc. Lond. A Math. 80/535 (1907) 45.
[103] D. Staack, B. Farouk, A. Gutsol, A. Fridman, Plasma Sources Sci. Technol. 17/2 (2008) 025013.
[104] A.v. Engel, Philos. Mag. 32/214 (1941) 417.
[105] L.D. Tsendin, Sov. Phys. Tech. Phys. 31 (1986) 169.
[106] Y.B. Golubovskii, S.H.a. Hawat, L.D. Tsendin, L.D. Tsendin, Sov. Phys. Tech. Phys. 32 (1987) 760.
[107] Y.B. Golubovskii, S.H. al Hawat, Sov. Phys. Tech. Phys. 32 (1987) 25.
[108] Y.B. Golubovskii, V.I. Kolobov, S.H.a. Hawat, Sov. Phys. Tech. Phys. 33 (1988) 1046.
[109] A. Bogaerts, J. Anal. At. Spectrom. 22/1 (2007) 13.
[110] D. Scott, A. Phelps, Phys. Rev. A 43/6 (1991) 3043.
[111] K. Rózsa, A. Gallagher, Z. Donkó, Phys. Rev. E 52/1 (1995) 913.
[112] A. Bogaerts, R. Gijbels, J. Vlcek, Spectrochim, Acta B: Atomic Spectros. 53 (1998) 1517–1526.
[113] A. Bogaerts, R. Gijbels, J. Anal. At. Spectrom. 13 (1998) 721.
[114] J. Remy, L. Biennier, F. Salama, Plasma Sources Sci. Technol. 12 (2003) 295.
[115] V.M. Tkaehenko, V.E. Tyutyunnik, Radiophys Quantum Electron. 16/11 (1973) 1759.
[116] J.E.H. Daughtrey, W.W. Harrison, Anal. Chem. 47/7 (1975) 1024.
[117] A. Bogaerts, R. Gijbels, V.V. Serikov, J. Appl. Phys. 87/12 (2000) 8334.
[118] S. Hashiguchi, M. Hasikuni, Jpn. J. Appl. Phys. 26/2 (1987) 271.
[119] A.S. Metel, A.I. Nastyukha, Radiophys Quantum Electron. 19/7 (1976) 1078.
[120] Karl H. Schoenbach, Ahmed El-Habachi, W. Shi, M. Ciocca, Plasma Sources Sci. Technol. 6 (1997) 468.
[121] H.-J. Han, Ph.D. Thesis, Naval postgraduate school, Monterey, CA, USA, 1989.
[122] K.H. Schoenbach, R. Verhappen, T. Tessnow, F.E. Peterkin, W.W. Byszewski, Appl. Phys. Lett. 68/1 (1996) 13.
[123] C.C. Van Voorhis, A.G. Shenstone, Rev. Sci. Instrum. 12/5 (1941) 257.
[124] H. Helm, Z. Naturforsch. A 27 (1923) 1812.
[125] J.P. Boeuf, L.C. Pitchford, J. Phys. D. Appl. Phys. 28 (1995) 2083.
[126] D. Söderström, H. Baránková, L. Bárdoš, J. Phys. Conf. Ser. 100/6 (2008) 062020.
[127] D.J. Sturges, H.J. Oskam, Physica 37 (1967) 457.
[128] E.M. van Veldhuizen, Ph.D. Thesis, Technische Hogeschool Eindhoven, The Netherlands, 1983.
[129] N. Baguer, A. Bogaerts, J. Appl. Phys. 98/3 (2005) 033303.
[130] G.G. Lister, J. Phys. D. Appl. Phys. 25 (1992) 1649.
[131] R.J. Carman, J. Phys. D. Appl. Phys. 22 (1989) 55.
[132] P. Gill, C. Webb, J. Phys. D. Appl. Phys. 10 (1977) 299.
[133] K. Kutasi, Z. Donko, J. Phys. D. Appl. Phys. 33 (2000) 1081.
[134] V.I. Kolobov, L.D. Tsendin, Plasma Sources Sci. Technol. 4 (1995) 551.
[135] D.J. Sturges, H.J. Oskam, J. Appl. Phys. 35/10 (1964) 2887.
[136] D.J. Sturges, H.J. Oskam, J. Appl. Phys. 37/6 (1966) 2405.
[137] D. Marić, N. Škoro, G. Malović, Z.L. Petrović, V. Mihailov, R. Djulgerova, J. Phys. Conf. Ser. 162 (2009) 012007.
[138] A.S. Metel, A.I. Nastyukha, Radiophys Quantum Electron. 19/12 (1976) 1884.
[139] L. Bardos, Surf. Coat. Technol. 86–87 (1996) 648.
[140] D. Mihailova, J.v. Dijk, G.J.M. Hagelaar, S. Karatodorov, P. Zahariev, M. Grozeva, J.J.A.M. van der Mullen, J. Phys. D. Appl. Phys. 45/16 (2012) 165201.
[141] G.J.M. Hagelaar, D.B. Mihailova, J. van Dijk, J. Phys. D. Appl. Phys. 43/46 (2010) 465204.
[142] G. Bánó, Z. Donkó, Plasma Sources Sci. Technol. 21/3 (2012) 035011.
[143] A. Bogaerts, A. Okhrimovskyy, N. Baguer, R. Gijbels, Plasma Sources Sci. Technol. 14/1 (2005) 191.
[144] L. Shang, Ouyang Ji-Ting, H. Feng, Chin. Phys. Lett. 27/6 (2010) 065201.

[145] M. Surendra, D.B. Graves, G.M. Jellum, Phys. Rev. A 41/2 (1990) 1112.
[146] N. Baguer, A. Bogaerts, R. Gijbels, Spectrochim. Acta B 57 (2002) 311.
[147] Lorente-Arcas, Plasma Phys. 14 (1972) 651.
[148] H. Bhuyan, E. Valderrama, M. Favre, H. Chuaqui, I. Mitchell, E. Wyndham, AIP Conf. Proc. 875 (2006) 401.
[149] C. Pérez, M.I.d.l. Rosa, K. Grützmacher, J. Phys. Conf. Ser. 227 (2010) 012039.
[150] M.I.d.l. Rosa, C. Pérez, K. Grützmacher, A.B. Gonzalo, J.A.d. Val, J. Phys. Conf. Ser. 227 (2010) 012038.
[151] S. Karatodorov, D. Mihailova, J. van Dijk, J. van der Mullen, M. Grozeva, J. Phys. Conf. Ser. 356 (2012) 012043.
[152] O.H. Chin, C.S. Wong, J. Fiz. Mal. 24/3 & 4 (2003) 107.
[153] R.M. Sankaran, Ph.D. Thesis, California Institute of Technology, CA, USA, 2004.
[154] R.R. Arslanbekov, A.A. Kudryavtsev, R.C. Tobin, Plasma Sources Sci. Technol. 7 (1998) 310.
[155] E.F. Kotp, A. AL-Ojeery, Aust. J. Basic Appl. Sci. 6/3 (2012) 817.
[156] H. Koch, J. Vac. Sci. Technol. A 9/4 (1991) 2374.
[157] V.V. Zhurin, Vac. Technol. Coat. (March 2009) 42 (vol. March).
[158] D.S. Belic, J. Lecointre, P. Defrance, J. Phys. B At. Mol. Opt. 43/18 (2010) 185203.
[159] B. I.G., The Physics and Technology of Ion Sources, Wiley, 2004.
[160] B. Zimmermann, F. Fietzke, H. Klostermann, J. Lehmann, F. Munnik, W. Möller, Surf. Coat. Technol. 212 (2012) 67.
[161] F. Howorka, J. Chem. Phys. 68/3 (1978) 804.
[162] F. Howorka, I. Kuen, J. Chem. Phys. 70/2 (1979) 758.
[163] I. Tanarro, V.J. Herrero, Plasma Sources Sci. Technol. 18/3 (2009) 034007.
[164] R.S. Pessoa, G. Murakami, G. Petraconi, H.S. Maciel, I.C. Oliveira, K.G. Grigorov, Braz. J. Phys. 36/2A (2006) 332.
[165] I.D. Boyd, J. Appl. Phys. 95/7 (2004) 3285.
[166] M. Turek, A. Drozdziela, K. Pyszniak, D. Maczka, B. Slowinski, Acta Phys. Pol. A 123/5 (2013) 843.
[167] W. Biel, M. Brose, M. David, H. Kempkens, J. Uhlenbusch, Plasma Phys. Controlled Fusion 39 (1997) 661.
[168] A.B. Gonzalo, C. Garca, K. Grützmacher, S. Mar, C. Pérez, M. Inmaculada de la Rosa, AIP Conf. Proc. 559 (2001) 221.
[169] N.M. Sisovic, G.L. Majstorovic, N. Konjevic, Eur. Phys. J. D 32/3 (2005) 347.
[170] N.M. Šišović, G.L. Majstorović, N. Konjević, Eur. Phys. J. D 41/1 (2006) 143.
[171] G.L. Majstorović, N.M. Šišović, N. Konjević, Plasma Sources Sci. Technol. 16/4 (2007) 750.
[172] S. Muhl, A. Mahmood, Diam. Relat. Mater. 9 (2000) 53.
[173] W. Lopez, S. Muhl, S.E. Rodil, Vacuum 83/5 (2009) 819.
[174] D.M. Goebe, K.K. Jameson, Ron M. Watkins, I. Katz, I.G. Mikellides, J. Appl. Phys. 98/11 (2005) 113302.
[175] M. Bessenrodt-Weberpae, J.U. Souw, H. Kempkens, Plasma Phys. Controlled Fusion 26/2 (1984) 409.
[176] D.J. Willins, R. Boyd, J. Phys. D. Appl. Phys. 6 (1973) 1447.
[177] L. Bardos, H. Barankova, Y.A. Lebedev, Surf. Coat. Technol. 163–164 (2003) 654.
[178] Takashi Masaki, Akihide Wada, Yukio Adachi, C. Hirose, Appl. Spectrosc. 42/1 (1988) 51.
[179] J. Greenan, C.M.O. Mahony, D. Mariotti, P.D. Maguire, Plasma Sources Sci. Technol. 20/2 (2011) 025011.
[180] C. Paduraru, Ph.D. Thesis, Stevens Institute of Technology, NJ, USA, 2004.
[181] A.E. Delahoy, S.Y. Guo, C. Paduraru, A. Belkind, J. Vac. Sci. Technol. A 22/4 (2004) 1697.
[182] A.S. Metel, Sov. Tech. Phys. 29/2 (1984) 141.
[183] S.V. Baranov, I.V. Baranova, N.P. Ivanov, Translated from Zh. Prildadnoi Spektroskopii 36/3 (1982) 357.
[184] L. Bardos, H. Barankova, S. Berg, Surf. Coat. Technol. 72 (1995) 174.
[185] V.G. Grechanyi, A.S. Metel, Sov. Phys. Tech. Phys. 27/3 (1982) 284.
[186] M. Krishnan, R.G. Jahn, W.F. von Jaskowsky, K.E. Clark, AIAA J. 15/9 (1977) 1217.
[187] A.D.G. Matthew, T. Domonkos, M.J. Patterson, AIAA J. 3345 (1998) 1.
[188] J.R. Wallace, D.F.S. Natusch, B.N. Colby, J.C.A. Evans, Anal. Chem. 48/1 (1976) 118.
[189] J.C. Williams, Jan-Yurn Kung, Yixin Chen, Xiangjun Cai, S.T. Griffin, Appl. Spectrosc. 49/11 (1995) 1705.
[190] D. Mihailova, J. van Dijk, M. Grozeva, G.J.M. Hagelaar, J.J.A.M. van der Mullen, J. Phys. D. Appl. Phys. 43/14 (2010) 145203.
[191] D. Korzec, M. Mildner, F. Hillemann, J. Engemann, Surf. Coat. Technol. 97 (1997) 759.
[192] L. Bardos, H. Barankova, S. Berg, Surf. Coat. Technol. 97 (1997) 723.
[193] H. Baránková, L. Bárdos, Surf. Coat. Technol. 205/17–18 (2011) 4169.
[194] D. Arbel, Z. Bar-Lev, J. Felsteiner, A. Rosenberg, Ya. Z. Slutsker, Phys. Rev. Lett. 8/1 (1997) 66.
[195] G. Pavelescu, M. Balkeanu, C. Popovici, J. Phys. D. Appl. Phys. 16 (1983) 2205.
[196] Jian-Jun Lai, Q.-M. Chen, J.-L. Qiu, J. Phys. D. Appl. Phys. 33 (2000) 1785.
[197] V.M. Tkachenko, V.B. Tyutyunnik, Sov. Phys. Tech. Phys. 17 (1972) 49.
[198] V.N. Glazunov, A.S. Metel, Sov. Phys. Tech. Phys. 26 (1981) 559.
[199] Shigeru Tanaka, Masato Akiba, Hiroshi Horiike, Y. Okumura, Y. Ohara, Rev. Sci. Instrum. 54 (1983) 1104.
[200] A. Semenov, Instrum. Exp. Tech. 36 (1993) 743.
[201] N. Gavrilov, G. Mesyats, G. Radkovski, V. Bersenev, Surf. Coat. Technol. 96 (1997) 81.
[202] Y. Ohtsu, J. Eguchi, Y. Yahata, Vacuum 101 (2014) 46.
[203] Y. Ohtsu, Y. Kawasaki, J. Appl. Phys. 113/3 (2013) 033302.
[204] Y. Ohtsu, N. Matsumoto, J. Vac. Sci. Technol. A 32/3 (2014) 031304.
[205] B. Zimmermann, F. Fietzke, W. Möller, Surf. Coat. Tech. 120-121 (1999) 704–708.
[206] X. Zhao, S. Chen, K. Chen, B. Chen, Plasma Sci. Technol. 16/1 (2014) 21.
[207] S. Komiya, J. Vac. Sci. Technol. 12/1 (1975) 589.
[208] S. Komiya, J. Vac. Sci. Technol. 13/1 (1976) 520.
[209] D.G. Williams, J. Vac. Sci. Technol. 11/1 (1974) 374.
[210] M. Nistor, P. Charles, M. Ganciu, M. Lamoureux, N.B. Mandache, Plasma Sources Sci. Technol. 11 (2002) 183.
[211] S. Walton, D. Leonhardt, R. Fernsler, Hollow Cathode Produced Electron Beams for Plasma Generation: Cathode Operation in Gas Mixtures, NRL/MR/6750-06-8992, 2006.
[212] V. Burdovitsin, E. Oks, Rev. Sci. Instrum. 70/7 (1999) 2975.
[213] G. Ciullo, A.N. Sharapa, A.V. Shemyakin, L. Tecchio, Rev. Sci. Instrum. 69/1 (1998) 59.
[214] M. Klihne, Hollow Cathode, Penning, and Electron-beam Excitation Sources, 1998.
[215] V. Dudnikov, J.P. Farrell, Rev. Sci. Instrum. 75/5 (2004) 1732.
[216] V.I. Gushenets, A.S. Bugaev, E.M. Oks, P.M. Schanin, A.A. Goncharov, Rev. Sci. Instrum. 81/2 (2010) 02B305.
[217] M. Turek, A. Droździel, K. Pyszniak, J. Sielanko, Vacuum 78/2–4 (2005) 649.
[218] M. Turek, A. Droździel, K. Pyszniak, S. Prucnal, Nucl. Instrum. Meth. A 654/1 (2011) 57.
[219] D. Zhechev, V.I. Zhemenik, S. Tileva, G.V. Mishinsky, N. Pyrvanova, Nucl. Instrum. Meth. B 204 (2003) 387.
[220] M. Benda, J. Vac. Sci. Technol. A 15/5 (1997) 2636.
[221] K. Nikolov, K. Köster, P. Kaestner, G. Bräuer, C.P. Klages, Vacuum 102 (2014) 31.
[222] N.V. Gavrilov, A.I. Men'shakov, Instrum. Exp. Tech. 54/5 (2011) 732.
[223] L. Shen, L. Wang, J.J. Xu, Surf. Coat. Technol. 228 (2013) S456.
[224] D.M. Goebel, K.K. Jameson, I. Katz, I.G. Mikellides, Phys. Plasmas 14/10 (2007) 103508.
[225] D.M. Goebel, I. Katz, Fundamentals of Electric Propulsion: Ion and Hall Thrusters, Jet Propulsion Laboratory, California Institute of Technology, 2008.
[226] S.D. Kovaleski, A Review of Testing of Hollow Cathodes for the International Space Station Plasma Contactor, NASA/TM-2001-211291 IEPC-01-271, 2001.
[227] S. Tashiro, M. Tanaka, M. Nakatani, K. Tani, M. Furubayashi, Surf. Coat. Technol. 201/9–11 (2007) 5431.
[228] A.K. Malik, P. Montarde, M.G. Haines, J. Phys. D. Appl. Phys. 33/16 (2000) 2037.
[229] H. Meyer, S. Klose, E. Pasch, G. Fussmann, Phys. Rev. E 61/4 (2000) 4347.
[230] S.A. Janjua, M. Ahmad, S.-u.-D. Khan, R. Khalid, A. Aleem, S. Ahmad, J. Phys. D. Appl. Phys. 40/5 (2007) 1416.
[231] A. Buuron, F. Koch, M. Nothe, H. Bolt, Surf. Coat. Technol. 116–119 (1999) 755.
[232] H. Morgner, M. Neumann, S. Straach, M. Krug, Surf. Coat. Technol. 108–109 (1998) 513.
[233] M. Tichý, Z. Hubička, M. Šícha, M. Čada, J. Olejníček, O. Churpita, L. Jastrabík, P. Virostko, P. Adámek, P. Kudrna, S. Leshkov, M. Chichina, Š. Kment, Plasma Sources Sci. Technol. 18/1 (2009) 014009.
[234] J.A. Thornton, J. Vac. Sci. Technol. 15/2 (1978) 171.
[235] W. Grimm, Spectrochim. Acta B 23 (1968) 443.
[236] Y.S. Kuo, J. Vac. Sci. Technol. A 4/3 (1986) 397.
[237] C.M. Horwitz, J. Vac. Sci. Technol. A 6/3 (1988) 1837.
[238] Annemie Bogaerts, Erik Neyts, Renaat Gijbels, J.v.d. Mullen, Spectrochim. Acta B 57 (2002) 609.
[239] A. Anders, Surf. Coat. Technol. 200/5–6 (2005) 1893.
[240] U. Helmersson, M. Lattemann, J. Bohlmark, A.P. Ehiasarian, J.T. Gudmundsson, Thin Solid Films 513/1–2 (2006) 1.
[241] R.J. Soukup, N.J. Ianno, J.L. Huguenin-Love, Sol. Energy Mater. Sol. Cells 91/15–16 (2007) 1383.
[242] L. Bárdos, H. Baránková, Vacuum 83/3 (2008) 522.
[243] L. Bárdos, H. Baránková, Thin Solid Films 518/23 (2010) 6705.
[244] O. Baranov, M. Romanov, S. Kumar, X.X. Zong, K. Ostrikov, J. Appl. Phys. 109/6 (2011) 063304.
[245] H. Kakiuchi, H. Ohmi, K. Yasutake, J. Vac. Sci. Technol. A 32/3 (2014) 030801.
[246] C.M. Horwitz, Appl. Phys. Lett. 43/10 (1983) 977.
[247] F. Fietzke, B. Zimmermann, Surf. Coat. Technol. 205/5 (2010) 1491.
[248] A. Belkind, S. Zarrabian, F. Engle, Met. Finish. (July 1996) 3.
[249] S.F. Brunatto, J.L.R. Muzart, J. Phys. D. Appl. Phys. 40/13 (2007) 3937.
[250] M. Quitzau, H. Kersten, Eur. Phys. J. D 66/2 (2012).
[251] X.B. Tian, H.F. Jiang, S.Q. Yang, Z.J. Luo, R.K.Y. Fu, P.K. Chu, Surf. Coat. Technol. 201/19–20 (2007) 8650.
[252] J.J. Cuomo, J. Vac. Sci. Technol. A 4/3 (1986) 393.
[253] D.F. Dawson-Elli, J. Vac. Sci. Technol. A 8/3 (1990) 1294.
[254] D.F. Dawson-Elli, J. Vac. Sci. Technol. A 9/4 (1991) 2442.
[255] Z. Wang, S.A. Cohen, Phys. Plasmas 6/5 (1999) 1655.
[256] J.W. Bradley, M. Cecconello, Vacuum 49/4 (1998) 315.
[257] Z. Wang, S.A. Cohen, J. Vac. Sci. Technol. A 17/1 (1999) 77.
[258] Yasunori Ohtsu, Yoshiki Yahata, Johji Kagami, Yasushi Kawashimo, T. Takeuchi, IEEE Trans. Plasma Sci. 41/8 (2013) 1856.
[259] V. Vyas, M.J. Kushner, J. Vac. Sci. Technol. A 24/5 (2006) 1955.
[260] S.A. Cohen, Z. Wang, A Hollow Cathode Magnetron (HCM), Princeton Plasma Physics Laboratory (PPPL), Princeton, NJ, 1998.
[261] G. Font, M.J. Kushner, Bull. Am. Phys. Soc. 44 (1999) 74.
[262] J.A. Thornton, J. Vac. Sci. Technol. 12/1 (1975) 93.
[263] J.A. Thornton, J. Vac. Sci. Technol. 12/4 (1975) 830.
[264] J.A. Thornton, D.P. Ferriss, Thin Solid Films 40/0 (1977) 365.
[265] J.A. Thornton, Z. Metallkd. 75/11 (1984) 847.
[266] David A. Glocker, Mark M. Romach, V.W. Lindberg, Surf. Coat. Technol. 146–147 (2001) 457.
[267] Th. Jung, T. Kalber, V.v.d. Heide, Surf. Coat. Technol. 86–87 (1996) 218.
[268] I. Ishii, Jpn. J. Appl. Phys. 26/6 (1987) L932.
[269] Abe Belkind, G.S. Tompa, Vac. Technol. Coat. (January 2008) 49.
[270] K. Ishii, S. Handa, H. Terauchi, Appl. Surf. Sci. 33–34 (1988) 1107.
[271] K. Ishii, J. Vac. Sci. Technol. A 7/2 (1989) 256.
[272] Th. Schurig, S. Menkel, Z. Quan, J. Beyer, B. Giittler, S. Knappe, H. Koch, Physica C 262 (1996) 89.
[273] K. Ishii, T. Ohba, T. Hara, Mater. Sci. Eng. A A217/218 (1996) 232.

[274] H. Barankova, L. Bardos, C. Nender, S. Berg, Surf. Coat. Technol. 86–87 (1996) 377.
[275] T. Kalber, T. Jung, Surf. Coat. Technol. 98 (1998) 1116.
[276] K. Ishii, J. Vac. Sci. Technol. A 16/2 (1998) 759.
[277] A. Hellmich, T. Jung, A. Kielhorn, M. Ribland, Surf. Coat. Technol. 98 (1998) 1541.
[278] H. Barankova, L. Bardos, Surf. Coat. Technol. 120–121 (1999) 704.
[279] M. Höfer, A. Jung, T. Jung, H.-U. Kricheldorf, F. Schmidt, 43th Annual Technical Conf. Proc. Society of Vacuum Coaters, 2000.
[280] J.-D. Suh, S.K. Han, K.Y. Kang, M.H. Kwak, IEEE Trans. Plasma Sci. 11/1 (2011) 3844.
[281] G. Pribil, Z. Hubička, R.J. Soukup, N.J. Ianno, J. Vac. Sci. Technol. A 19/4 (2001) 1571.
[282] Z. Hubick, G. Pribil, R.J. Soukup, N.J. Ianno, Surf. Coat. Technol. 160 (2002) 114.
[283] A.A. Pradhan, S.I. Shah, K.M. Unruh, Rev. Sci. Instrum. 73/11 (2002) 3841.
[284] C. Paduraru, A. Belkind, J.L.K. Becker, A. Delahoy, S.Y. Guo, 46th Annual Technical Conf. Proc. Society of Vacuum Coaters, 2003.
[285] A.E. Delahoy, S.Y. Guo, J. Vac. Sci. Technol. A 23/4 (2005) 1215.
[286] S. Tang, U. Schulz, Surf. Coat. Technol. 204/6–7 (2009) 1087.
[287] L. Bardos, H. Barankova, L.E. Gustavssona, D.G. Teer, Surf. Coat. Technol. 177–178 (2004) 651.
[288] M. Birkholz, U. Albers, T. Jung, Surf. Coat. Technol. 179/2–3 (2004) 279.
[289] C.M. Li, H. Lei, Y.J. Tang, J.S. Luo, W. Liu, Z.M. Chen, Nanotechnology 15/12 (2004) 1866.
[290] R.J. Soukup, N.J. Ianno, G. Pribil, Z. Hubick, Surf. Coat. Technol. 177–178 (2004) 676.
[291] R.J. Soukup, N.J. Ianno, S.A. Darveau, C.L. Exstrom, Sol. Energy Mater. Sol. Cells 87/1–4 (2005) 87.
[292] J.S. Schrader, J.L. Huguenin-Love, R.J. Soukup, N.J. Ianno, C.L. Exstrom, S.A. Darveau, R.N. Udey, V.L. Dalal, Sol. Energy Mater. Sol. Cells 90/15 (2006) 2338.
[293] H. Jacobsen, H.-J. Quenzer, B. Wagner, K. Ortner, T. Jung, MEMS 2006, 2006.
[294] K. Ortner, D. Koeßler, T. Jung, H. Jacobsen, H.-J. Quenzer, Plasma Process. Polym. 4/S1 (2007) S134.
[295] H. Jacobsen, H.J. Quenzer, B. Wagner, K. Ortner, T. Jung, Sensors Actuators A Phys. 135/1 (2007) 23.
[296] M. Bedenbecker, R. Bandorf, H. Luethje, G. Braeuer, H.H. Gatzen, Microsyst. Technol. 12/7 (2006) 655.
[297] R. Bandorf, A. Bloche, K. Ortner, H. Lüthje, T. Jung, Plasma Process. Polym. 4/S1 (2007) S129.
[298] H.A.H. Sakuma, K. Ishii, J. Magn. 11/3 (2006) 103.
[299] H. Aoshima, H. Suzuki, H. Sakuma, K. Ishii, J. Appl. Phys. 105/7 (2009) 07B519.
[300] C.-Y. Cheng, F.C.-N. Hong, Thin Solid Films 498/1–2 (2006) 206.
[301] F.O. de Araújo, E.O. de Almeida, C. Alves, J.A.P. da Costa, T. Dumelow, Surf. Coat. Technol. 201/6 (2006) 2990.
[302] H. Sakuma, K. Ishii, J. Magn. Magn. Mater. 321/7 (2009) 872.
[303] H.K. Jonathan, L. Van Noord, Heather K. McEwen, 29th International Electric Propulsion Conference, 2006.
[304] V.A. Lisovskiy, A. Bogodielny, V.D. Yegorenkov, V.N.K. Kharkov, Probl. At. Sci. Technol. (BAHT) 4/86 (2013) 144.
[305] H. Sakuma, Y. Watanabe, K. Aramaki, K.S. Yun, K. Ishii, Y. Ikeda, H. Kondo, Mater. Sci. Eng. B Solid 173/1–3 (2010) 7.
[306] H. Sakuma, S. Sakamoto, A. Naoi, Y. Saito, K. Ishii, J. Vac. Sci. Technol. A 30/6 (2012) 061604.
[307] N. Oka, M. Watanabe, K. Sugie, Y. Iwabuchi, H. Kotsubo, Y. Shigesato, Thin Solid Films 532 (2013) 1.
[308] Z. Hubička, Š. Kment, J. Olejníček, M. Čada, T. Kubart, M. Brunclíková, P. Kšírová, P. Adámek, Z. Remeš, Thin Solid Films 549 (2013) 184.
[309] I. Pilch, D. Söderström, M.I. Hasan, U. Helmersson, N. Brenning, Appl. Phys. Lett. 103/19 (2013) 193108.
[310] R. Perekrestov, P. Kudrna, M. Tichý, WDS'13 Proceedings of Contributed Papers, 2013. 139.
[311] A. Perez, A.T. Luna, S. Muhl, J. Phys. D. Appl. Phys. 46/50 (2013) 505303.
[312] A. Saxena, P. Kumar, S. Banerjee, K.P. Subramanian, B. Bapat, Spectrosc. Lett. 47/2 (2014) 114.
[313] M.L. Bardos, Czechoslov. J. Phys. 35 (1985) 1437.
[314] B. Singh, O.R. Mesker, A.W. Levine, Y. Arie, Appl. Phys. Lett. 52/20 (1988) 1658.
[315] F. Jansen, J. Vac. Sci. Technol. A 7/6 (1989) 3176.
[316] M.V. Bazylenko, M. Gross, P.M. Allen, P.L. Chu, IEEE Trans. Plasma Sci. 7/7 (1995) 774.
[317] M.V. Bazylenko, M. Gross, P.L. Chu, D. Moss, Electron. Lett. 32/13 (1996) 1198.
[318] J. Canning, D. Moss, M. Aslund, M. Bazylenko, Electron. Lett. 34/4 (1998) 366.
[319] D. Korzec, J. Engemann, M. Mildner, K.-P. Ningel, 0. Borgmeier, D. Theirich, Surf. Coat. Technol. 93 (1997) 128.
[320] K.P. Ningel, D. Theirich, J. Engemann, Surf. Coat. Technol. 98 (1998) 1142.
[321] M. Nakamura, D. Korzec, T. Aoki, J. Engemann, Y. Hatanaka, Appl. Surf. Sci. 175–176 (2001) 697.
[322] G. Fedosenko, D. Korzec, J. Engemann, D. Lyebyedyev, H.-C. Scheer, Thin Solid Films 406 (2002) 275.
[323] G. Fedosenkoa, A. Schwabedissen, J. Engemann, E. Braca, L. Valentini, J.M. Kenny, Diam. Relat. Mater. 11 (2002) 1047.
[324] R. Wei, C. Rincon, T.L. Booker, J.H. Arps, Surf. Coat. Technol. 188–189 (2004) 691.
[325] G. Capote, L.G. Jacobsohn, M.D. Michel, C.M. Lepienski, A.L. Vieira, D.F. Franceschini, Diam. Relat. Mater. 16/3 (2007) 616.
[326] H.F. Jiang, X.B. Tian, S.Q. Yang, R.K.Y. Fu, P.K. Chu, J. Vac. Sci. Technol. A 26/5 (2008) 1149.
[327] S. Saloum, M. Naddaf, Vacuum 82/1 (2007) 50.
[328] D. Lusk, M. Gore, W. Boardman, T. Casserly, K. Boinapally, M. Oppus, D. Upadhyaya, A. Tudhope, M. Gupta, Y. Cao, S. Lapp, Diam. Relat. Mater. 17/7–10 (2008) 1613.
[329] J. Ni, W. Wu, X. Ju, X. Yang, Z. Chen, Y. Tang, Thin Solid Films 516/21 (2008) 7422.
[330] J. Ni, X.P. Hao, Adv. Mater. Res. 538–541 (2012) 124.
[331] C. Wachtendorf, C. Herweg, M. Daeuber, J. Benedikt, A. von Keudell, J. Phys. D. Appl. Phys. 42/9 (2009) 095205.
[332] W.-D. Wu, J. Ni, X.-M. Wang, X.-D. Yang, Z.-M. Chen, Y.-J. Tang, Vacuum 83/11 (2009) 1397.
[333] D. Lusk, T. Casserly, M. Gupta, K. Boinapally, Y. Cao, R. Ramamurti, P. Desai, Plasma Process. Polym. 6/S1 (2009) S429.
[334] K.-C. Liu, H.-L. Cheng, J.-R. Tsai, Y.-L. Chiang, Y.-C. Hsieh, D.-J. Jan, Thin Solid Films 518/22 (2010) 6195.
[335] P. Dimitrakellis, E. Amanatides, D. Mataras, D.E. Rapakoulias, J. Phys. Conf. Ser. 275 (2011) 012014.
[336] J. Schindhelm, M. Giza, K. Nikolov, N. Weiher, B. Schuhmacher, C.P. Klages, Surf. Coat. Technol. 205 (2011) S137.
[337] A. Michael, A. Al Hafiz, T. Puzzer, C.Y. Kwok, Sensors Actuators A Phys. 178 (2012) 110.
[338] H. Pedersen, P. Larsson, A. Aijaz, J. Jensen, D. Lundin, Surf. Coat. Technol. 206/22 (2012) 4562.
[339] V.L. Bukhovets, A.E. Gorodetsky, R.K. Zalavutdinov, A.P. Zakharov, High Energy Chem. 47/2 (2013) 67.
[340] S. Günther, M. Fahland, J. Fahlteich, B. Meyer, S. Straach, N. Schiller, Thin Solid Films 532 (2013) 44.
[341] D. Lundin, H. Pedersen, Phys. Procedia 46 (2013) 3.
[342] X. Pang, H. Peng, H. Yang, K. Gao, X. Wu, A.A. Volinsky, Thin Solid Films 534 (2013) 226.
[343] E. Goldenberg, C. Ozgit-Akgun, N. Biyikli, A. Kemal Okyay, J. Vac. Sci. Technol. A 32/3 (2014) 031508.
[344] C. Ozgit-Akgun, E. Goldenberg, A.K. Okyay, N. Biyikli, J. Mater. Chem. C 2/12 (2014) 21.
[345] E.F. Shevchenko, V.A. Tarala, M.Y. Shevchenko, A.A. Titarenko, Adv. Mater. Sci. Eng. 2014 (2014) 1.
[346] R.A. Baragiola, Philos. Trans. R. Soc. Lond. A 362 (2004) 29.
[347] D.M. Mehs, T.M. Niemczyk, Appl. Spectrosc. 32/3 (1978) 269.
[348] S.P. Wolsky, E.J. Zdanuk, Phys. Rev. 121/2 (1961) 374.
[349] M.R. Nakles, M.Sc.Thesis, Virginia Polytechnic Institute and State University, VA, USA, 2004.